*applied sciences*

MDPI

*Article*

# Finite Element Modelling of Mandibular Fracture Fixation: Comparative Assessment of Miniplate Configurations and Mechanical Stability †

**Andrii Kondratiev [1,2,3,*], Vladislav Demenko [4], Vitaly Miroshnikov [4], Larysa Linetska [5] and Igor Linetskiy [6]**

1 Institute of Lightweight Engineering and Polymer Technology, TUD Dresden University of Technology, 01069 Dresden, Germany
2 Murray Edwards College, University of Cambridge, Huntingdon Road, Cambridge CB3 0DF, UK
3 Department of Materials Science and Engineering of Composite Structures, O.M. Beketov National University of Urban Economy in Kharkiv, Chornohlazivska Str. 17, 61002 Kharkiv, Ukraine
4 Department of Aircraft Strength, National Aerospace University "Kharkiv Aviation Institute", Vadym Manko Str. 17, 61070 Kharkiv, Ukraine; v.demenko@khai.edu (V.D.); v.miroshnikov@khai.edu (V.M.)
5 Department of Rehabilitation Medicine, National Technical University Kharkiv Polytechnic Institute, Kyrpychova Str. 2, 61002 Kharkiv, Ukraine; larisa.linetska@gmail.com
6 Department of Oral and Maxillofacial Surgery, General University Hospital in Prague, U Nemocnice 499/2, 128 08 Prague, Czech Republic; igor.linetskiy@gmail.com
* Correspondence: andrii.kondratiev@mailbox.tu-dresden.de
† This article is a revised and expanded version of our paper published in Kondratiev, A.; Sutcliffe, M.; Demenko, V.; Linetskiy, I.; Yefremov, O.; Linetska, L. Efficiency of Miniplates Fixation in Mandibular Oblique Fractures. In Proceedings of the 2024 IEEE 5th KhPI Week on Advanced Technology (KhPIWeek), Kharkiv, Ukraine, 7–11 October 2024, pp. 1–6. https://doi.org/10.1109/KhPIWeek61434.2024.10878063.

## Abstract

**Background/Objectives:** Stable fixation of mandibular fractures is essential for maintaining bone fragment alignment and providing a favorable mechanical environment for fracture healing. The geometry of titanium osteosynthesis miniplates influences load transfer, interfragmentary motion, and the mechanical stability of fixation. This study aimed to evaluate the biomechanical performance of two titanium miniplate configurations used for mandibular fracture fixation through detailed finite element analysis. **Methods:** A three-dimensional finite element model of a fractured mandible was developed from computed tomography data, incorporating distinct cortical and cancellous bone regions. Two fixation configurations incorporating titanium miniplates (27 × 2.5 × 1.25 mm and 20.5 × 3.5 × 1.25 mm) and titanium screws were investigated under simulated postoperative masticatory loading. The modelling approach incorporated detailed screw geometry, screw pretension, nonlinear contact interactions, and local mesh refinement. Fixation performance was evaluated in terms of displacement, interfragmentary gap opening and sliding, and stress distribution in the bone–plate–screw system. **Results:** The shorter, wider miniplate configuration demonstrated lower reported displacement (0.628 mm versus 0.728 mm), reduced cortical bone gap opening (0.13 mm versus 0.15 mm), and smaller interfragmentary sliding (0.06 mm versus 0.11 mm) compared with the longer, narrower configuration. Maximum von Mises stresses in the fixation screws decreased from 250 to 220 MPa. Both configurations exhibited stress concentrations near the fixation regions, with the superior plate subjected predominantly to tensile loading, consistent with established osteosynthesis principles. **Conclusions:** The numerical results demonstrate that miniplate geometry affects load transfer and mechanical stability in mandibular fracture fixation. For the investigated loading and fixation conditions, the shorter, wider configuration provided more effective restriction of interfragmentary motion and reduced screw stresses. These findings support the biomechanical assessment of titanium osteosynthesis devices and may influencethe selection of fixation configurations in oral and maxillofacial surgery.

Check for updates

Academic Editors: Żaneta Anna Mierzejewska, Michał Krasowski and Leszek Szalewski

Received: 9 October 2026
Revised: 22 November 2026
Accepted: 23 November 2026
Published: 28 November 2026

**Copyright:** © 2026 by the authors. Licensee MDPI, Basel, Switzerland. This article is an open access article distributed under the terms and conditions of the Creative Commons Attribution (CC BY) license.

**Keywords:** mandibular fracture; titanium miniplates; osteosynthesis; finite element analysis; biomechanical stability; interfragmentary motion; oral and maxillofacial surgery

## 1. Introduction

The treatment of mandibular fractures presents a significant challenge in maxillofacial surgery [1]. Over the past two decades, the incidence of maxillofacial trauma has risen from 3.2% to 5.8% [2,3], with mandibular fractures comprising 75% to 95% of all facial bone injuries [4]. Patients suffering from these fractures constitute approximately 20% of hospital admissions in maxillofacial units, predominantly within the working-age demographic (18–40 years) [5].

Despite advancements in osteosynthesis techniques and the availability of various fixation devices, complication rates remain substantial, ranging from 12% to 40% [6,7]. A major contributor to these complications is inadequate fixation of bone fragments, which can result in displacement, loss of anatomical integrity, and impaired functionality of the masticatory system [8]. Additionally, improper realignment of fragments may further damage bone tissue, complicating the healing process [9].

Modern osteosynthesis techniques, particularly the use of miniplates, are designed to enhance fracture stabilization by ensuring optimal repositioning and rigid fixation of bone fragments [10]. Miniplates are widely used in maxillofacial surgery due to their small size, adaptability, ease of placement, and accessibility via an intraoral approach [11,12]. Their benefits include reduced complication rates, prevention of malocclusion, avoidance of temporomandibular joint dysfunction, and improved aesthetic outcomes [13].

For successful osseointegration, fixation devices are fabricated from biocompatible materials such as titanium and its alloys [14]. These materials offer excellent mechanical properties, corrosion resistance, and hypoallergenic characteristics, making them highly effective in mandibular fracture treatment [15].

Despite extensive research, optimal surgical approaches for mandibular fractures remain a topic of debate. Effective treatment strategies must integrate repositioning and immobilization of bone fragments, with the selection of an appropriate fixation method depending on multiple factors [16]. Addressing these challenges requires an interdisciplinary approach that merges biomechanics and computational modelling [17].

In recent years, the reliance on empirical methods in maxillofacial surgery and traumatology has been gradually replaced by advanced computational approaches [18]. Among these, finite element analysis (FEA) has emerged as a highly effective technique for evaluating and optimizing fixation systems [19]. This simulation-based method enables precise replication of the mechanical behavior of biological structures under functional loading, offering unparalleled insights into the biomechanical performance of fixation devices [20,21]. FEA has proven to be a powerful tool in addressing both theoretical and practical challenges in maxillofacial surgery [22]. By allowing for a detailed assessment of stress distribution, deformation, and fixation stability, this approach enhances treatment planning and improves patient outcomes [23]. The growing interest in this field is reflected in the increasing number of research publications dedicated to refining computational models and validating their clinical relevance [24,25]. As a result, FEA continues to play a crucial role in advancing surgical techniques and optimizing patient-specific treatment strategies [26,27].

A comprehensive review conducted in [28] employed FEA to assess the biomechanical performance of titanium-based biometallic alloys for fracture fixation and tissue rehabilitation. The study highlighted the advantages of these materials, including biocompatibility, high mechanical strength, and resistance to degradation. However, this review primarily

compiles findings from the existing literature without delving into specific fixation strategies, postoperative load variations, or advanced contact modeling techniques.

In [29], a FEA investigation explored titanium mandible plates reinforced with graphene nanoplatelets, reporting a 10–22% reduction in stress concentration. While this study focused on optimizing material properties, it employed a simplified representation of bone structures and fixation mechanics, thereby limiting its ability to assess biomechanical stability under functional loads.

The study in [30] compared the biomechanical performance of magnesium and titanium fixation plates for unilateral mandibular angle fractures using FEA. Three plate configurations were evaluated—a straight plate with an interval, a straight plate without an interval, and a circular bar—under masticatory loads ranging from 100 to 500 N. The findings suggested that plates could sustain loads within their compressive yield limit. However, this study assumed a homogeneous bone structure without differentiating cortical and cancellous bone properties. Additionally, the absence of detailed contact analysis between screws, plates, and bone structures limited its accuracy in modeling fixation mechanics.

A separate FEA study in [31] analyzed various mandibular fracture fixation techniques and validated the computational results through mechanical testing on polymeric mandible models. The study demonstrated that stress distribution was primarily concentrated in miniplates, with higher von Mises stress observed in inferior plate fixation compared to superior border fixation. Furthermore, two-plate configurations significantly reduced displacement and enhanced overall stability. Despite these findings, the reliance on polymeric models simplified the bone's mechanical response, making it less representative of real clinical conditions.

Another FEA study in [32] assessed the biomechanical performance of mandibular fracture fixation devices under different clenching tasks and fracture scenarios. By modeling both healthy and fractured mandibles, the study examined stress distribution in fixation plates and strain patterns at the fracture site. The results indicated that the highest mechanical loads were concentrated near the fracture line, with stress peaks forming around screw insertions and plate bending points. However, this research did not incorporate patient-specific variations and used simplified material properties. Additionally, it did not explore multiple fixation designs or their impact on stress shielding, which are crucial for optimizing fixation strategies.

In [33], researchers conducted an FEA comparison of miniplate and reconstruction plate fixation in the treatment of bilateral parasymphysis mandibular fractures. The study simulated functional loading (120 N in the molar region and 62.5 N in the incisor region), demonstrating that miniplates resulted in smaller interfragmentary gaps and reduced sliding displacement compared to reconstruction plates, indicating superior stability. However, the study was limited to static loading conditions and did not account for postoperative load variations or advanced contact mechanics, both of which are essential for understanding the long-term biomechanical performance of fixation devices.

A novel V-shaped miniplate designed for simultaneous reduction and fixation of mandibular fractures was evaluated in [34]. The study compared this design with a conventional linear miniplate, analyzing their biomechanical response under postoperative masticatory loading conditions. While the research provided valuable insights into plate geometry, it employed simplified material properties, which could influence the accuracy of stress predictions.

In [35], an FEA study investigated the biomechanical feasibility of shortened additively manufactured mandibular reconstruction plates versus conventional long plates. The results suggested that combining long and short plates enhanced fixation stability, reducing maximum tensile stress by 6.3% and relative displacement by 41.4%, while maintaining

bone segment dislocation below 42.1 µm. However, the study relied on a simplified bone structure model and did not assess postoperative load variations, limiting its applicability in clinical settings.

A patient-specific Ti6Al4V mandibular reconstruction plate was analyzed in [36] using FEA to investigate stress distribution. The results revealed significant stress concentrations around screw holes and near the resection site, with the maximum tensile stress reaching 392.6 MPa, identifying critical regions prone to mechanical failure. Additionally, the study confirmed that plate design plays a crucial role in stress gradients, particularly in regions subjected to bending and torsional forces. However, this work primarily focused on stress behavior after fixation and did not explore alternative fixation strategies or plate geometry optimization.

A FEA study in [37] compared the biomechanical performance of locking and non-locking miniplates in mandibular fracture fixation. The results demonstrated that locking plates reduced stress concentrations and improved resistance to displacement, making them a more mechanically stable option. However, the study simplified the bone structure model, did not differentiate between cortical and cancellous bone, and lacked a detailed analysis of contact mechanics between screws, plates, and bone.

Finally, in our previous conference study [38], FEA was utilized to analyze the biomechanical behavior of osteosynthesis systems under postoperative muscle loading, with particular attention to controlled micromovements in alveolar crest reconstruction. The findings highlighted the importance of maintaining micromovements within physiologically acceptable limits, while excessive stress concentrations mightcompromise fixation stability. However, that study primarily focused on selected biomechanical aspects without a comprehensive comparison of stress distributions across different fixation configurations.

The present study builds upon and substantially extends the earlier conference contribution [38] by incorporating a more detailed assessment of mandibular fracture fixation mechanics. The expanded scope of the investigation is reflected in the revised title of the manuscript. In particular, the study addresses several limitations of previous FEA investigations, including simplified representations of bone structure, postoperative loading conditions, and contact interactions. The objective is to employ advanced finite element modelling techniques to compare the mechanical response of different fixation configurations, evaluate stress distributions and interfragmentary displacements, and identify factors influencing the mechanical stability of mandibular fracture fixation.

## 2. Materials and Methods

Mandibular morphology was evaluated using computed tomography (CT) scans of an anonymized patient (Figure 1). The CT dataset used for the reconstruction of the three-dimensional mandibular geometry was obtained from pre-existing clinical imaging records and retrospectively used for the present finite element analysis. The dataset was anonymized prior to its use in the present study. The Digital Imaging and Communications in Medicine (DICOM) data were processed using 3D Slicer software. The mandibular bone was segmented from the CT images, and the resulting three-dimensional geometry was exported in stereolithography (STL) format for further processing.

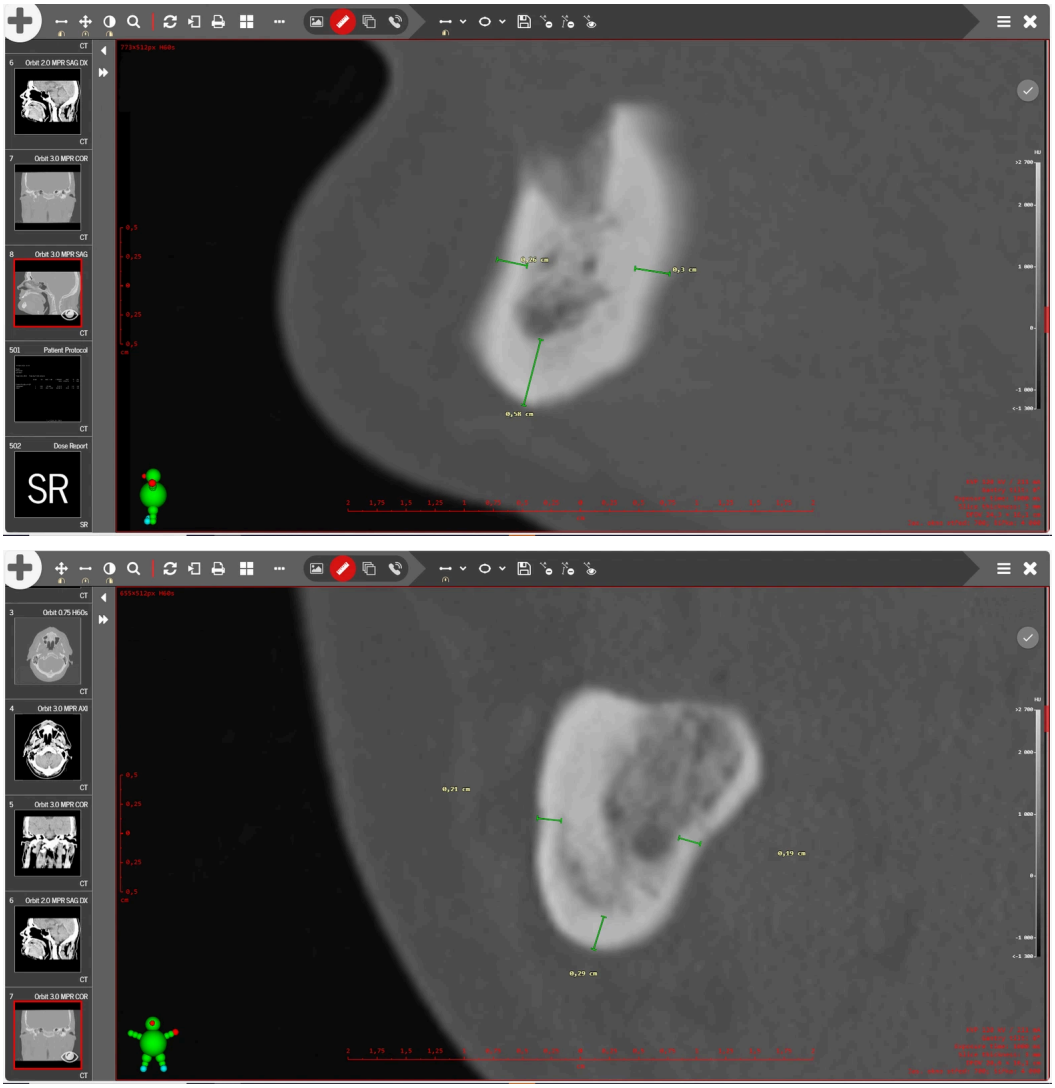

**Figure 1.** Representative CT scans utilized for mandibular morphology assessment.

The model was defined using an X, Y, Z coordinate system, with the origin positioned equidistantly between the left and right condylar processes on the X–Y plane. The *X*-axis represented the medio-lateral direction, the *Y*-axis denoted the superior–inferior direction, and the *Z*-axis indicated the anterior–posterior direction (Figure 2). Teeth were excluded from the mechanical strength/stiffness analysis to streamline the modeling process.

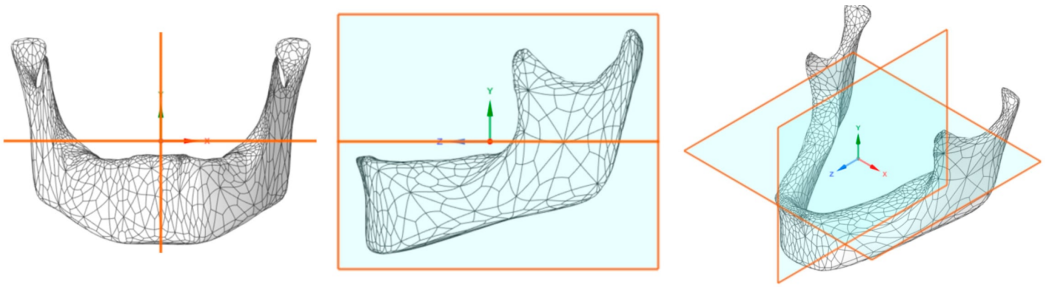

**Figure 2.** 3D model generated from CT images.

The STL model was processed using Ansys Mechanical SpaceClaim 2021 R2 (Ansys, Inc., Canonsburg, PA, USA) , where the triangulated surface geometry was converted into a CAD-compatible model and exported in the Standard for the Exchange of Product Model

Data (STEP) format. The resulting STEP model was subsequently imported into ANSYS DesignModeler for further geometric processing and simulation of a mandibular fracture scenario.

Geometric properties of cortical and cancellous bone were determined based on established methodologies [39,40] (Figure 3). Medical imaging software(Dicompass Gateway WebViewer, MEDORO s.r.o., Pardubice, Czech Republic) was used to quantify local cortical shell thickness.

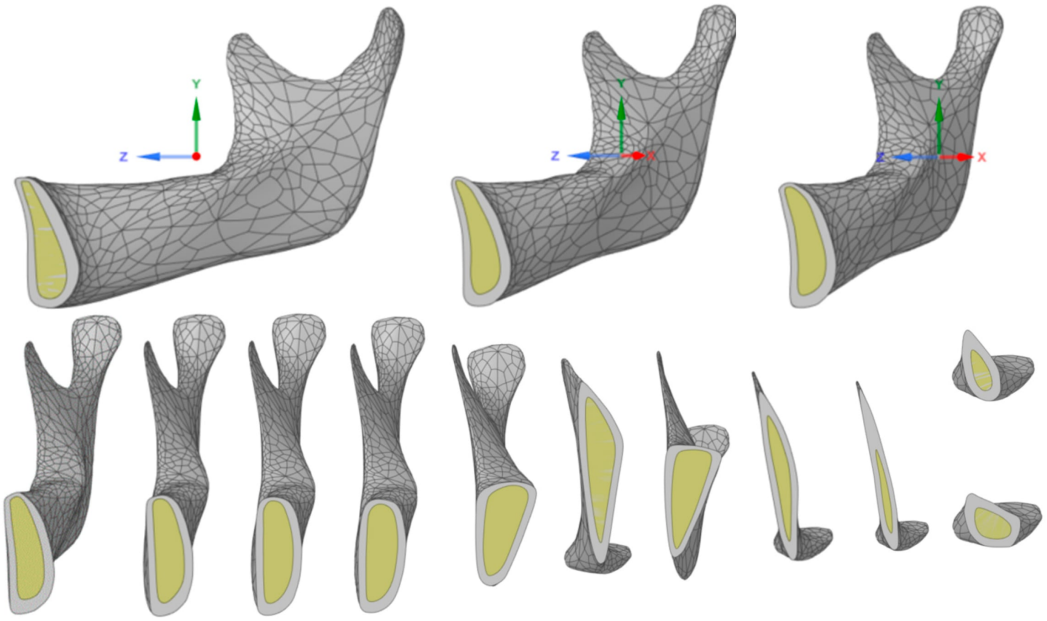

**Figure 3.** 3D representation of cortical and cancellous bone structures in selected sections(grey—cortical bone; yellow—cancellous bone).

An initial interfragmentary gap of approximately 0.5 mm was introduced to represent incomplete apposition of the fracture surfaces following anatomical reduction. This value is consistent with previous finite element studies of mandibular fracture fixation, in which a 0.5 mm gap was explicitly adopted [41,42].

Based on AO guidelines [43] and Champy's osteosynthesis principles [44], the mandible's alveolar region was identified as the tension zone, while the lower mandibular border was classified as the compression zone. The exact locations of these zones varied depending on the force direction. This information facilitated the definition of optimal osteosynthesis lines for internal fixation.

To stabilize the fracture, two configurations of commercially available titanium osteosynthesis miniplates were considered, based on the MatrixMANDIBLE Plate and Screw System (DePuy Synthes (Johnson & Johnson), West Chester, PA, USA) described in the manufacturer's product catalogue [45]. The selected configurations differed in length and width: 27 × 2.5 × 1.25 mm and 20.5 × 3.5 × 1.25 mm (Figure 4).

Two four-holed titanium miniplates were positioned for optimal fracture stabilization. The first plate was placed 4 mm from the alveolar crest and fixed with 2 mm screws. The second plate was secured along the lower mandibular border (Figure 5). Proper adaptation of the plates ensured precise bone alignment, preventing slippage and misalignment while optimizing load-sharing during osteosynthesis.

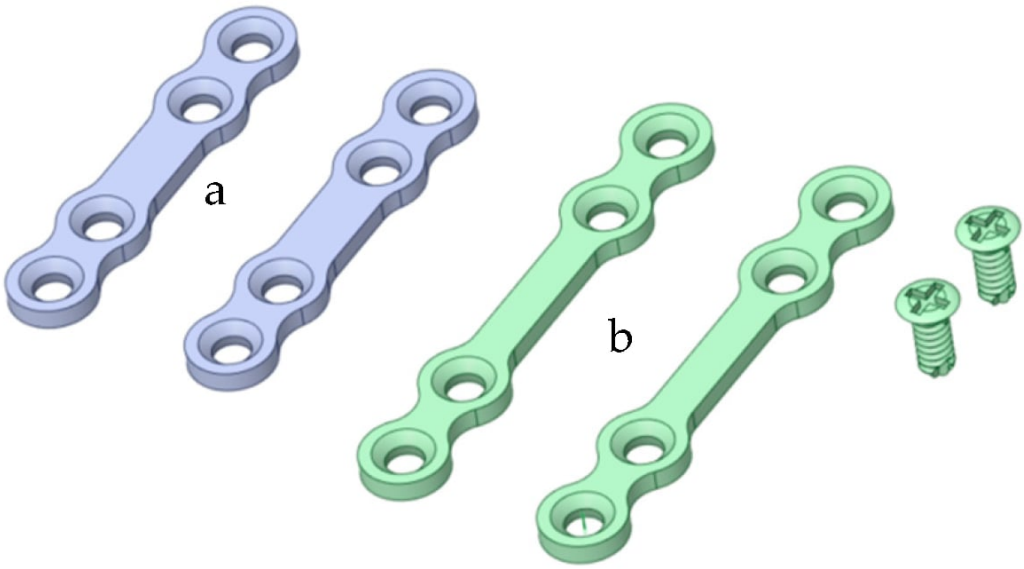


**Figure 4.** Miniplates and screws used for fixation: (**a**) 20.5 × 3.5 × 1.25 mm; (**b**) 27 × 2.5 × 1.25 mm.

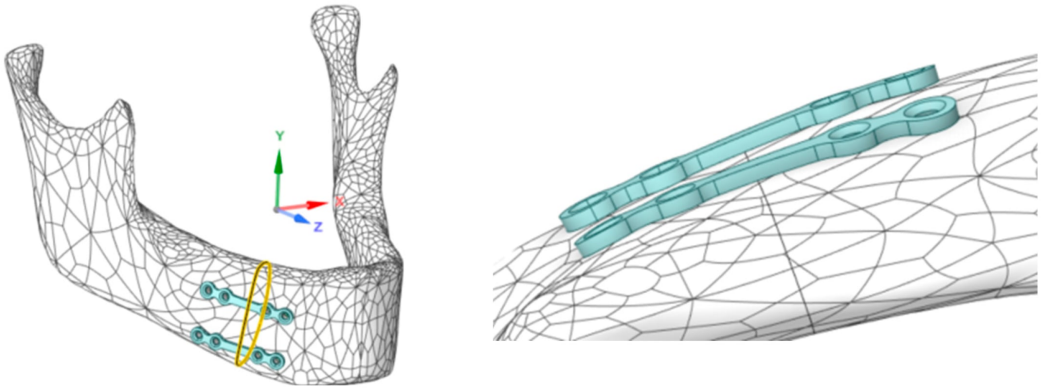


**Figure 5.** Mandibular fracture with fixation devices in place. The yellow circle highlights the region of the fracture plane.

The fracture was modelled as rough, with no significant serrations, and bone properties were assumed isotropic. Contact interactions were established between the screws, plates, and mandible, incorporating pre-tensioned screws to enhance fixation stability.

Frictional contact with a coefficient of friction of 0.3 was defined at two interfaces: between the opposing bone surfaces at the fracture site and between the titanium miniplates and the mandibular bone. The coefficient was adopted as a modelling assumption, informed by the frictional contact approach used in previous finite element investigations of mandibular fracture fixation [34].

The opposing fracture surfaces were allowed to separate, close, and slide relative to each other. Thus, the initially introduced geometric gap did not impose a constant separation between the bone fragments during loading.

A reference value for screw pretension was estimated using a separate three-dimensional finite element simulation of axial screw pull-out from cortical bone. Unlike the main mandibular model, in which bone was assumed to be linear elastic, the auxiliary simulation employed a bilinear elastoplastic material model with isotropic hardening for cortical bone, characterized by a Young's modulus of 13.7 GPa, a Poisson's ratio of 0.30, a yield stress of 50 MPa, and a tangent modulus of 10 MPa. The model explicitly represented the threaded screw–bone interface and was subjected to displacement-controlled axial pull-out

loading. The predicted force–displacement response indicated the onset of pronounced localized plastic deformation around the screw threads at approximately 325 N, followed by a maximum axial resistance of approximately 345 N. Applying a nominal safety factor of 2.5 yielded an estimated reference limit of 138 N. A slightly lower value of 130 N per screw was subsequently adopted as a modelling assumption for the global mandibular analysis. This value represents a numerically motivated reference preload rather than an experimentally validated screw-tightening force.

In the global mandibular model, the fixation screws were represented by equivalent beam connections with a diameter of 1.4 mm, corresponding to the minor diameter of the threaded section. Screw pretension was introduced using the ANSYS Bolt Pretension condition. The loading procedure comprised two sequential steps: first, the prescribed pretension was established; subsequently, the pretension condition was locked and the masticatory muscle forces were applied. For local stress analysis, a refined three-dimensional model explicitly representing the threaded screw geometry and frictional contact interactions was employed.

According to the manufacturer's specifications for the MatrixMANDIBLE Plate and Screw System [45], the fixation plates are manufactured from commercially pure titanium, whereas the fixation screws are manufactured from a titanium alloy (Ti6Al4V). These material specifications were considered when defining the mechanical properties of the fixation components in ANSYS. Different linear elastic material properties were assigned to the plates and screws, as summarized in Table 1. The material behavior was defined using the Young's modulus and Poisson's ratio, based on the literature values [20,46,47].

**Table 1.** Mechanical properties of the selected materials.

| Materials | Young's Modulus, GPa | Poisson's Ratio |
|---|---|---|
| Cortical bone | 13.70 | 0.30 |
| Cancellous bone | 1.37 | 0.30 |
| Pure titanium | 105 | 0.34 |
| Titanium alloy Ti6Al4V | 104.47 | 0.36 |

Four primary masticatory muscles (masseter, temporalis, medial pterygoid, and lateral pterygoid) were simulated, each exerting functional forces in distinct directions.

To approximate postoperative loading conditions, the reference muscle forces associated with clenching were reduced to 60% of their original magnitudes (i.e., a 40% reduction) [48]. Additional muscle-specific and side-dependent scaling factors, as reported in Table 2 [49], were applied to account for differences in muscle activation. Consequently, the effective applied forces were lower than 60% of the corresponding reference forces for muscle groups with scaling factors below unity. These loading conditions represent an assumed postoperative muscle activation scenario rather than experimentally measured patient-specific muscle forces.

Each muscle group was assigned unit vectors and a scaling parameter based on the specific side of the mandible where clenching forces were applied. The positioning of muscle force applications and fixed supports was determined through prior research [49].

The muscle force application points were positioned on both sides of the mandible, with the force vectors oriented according to the anatomical arrangement of the corresponding muscle groups. As shown in Table 2, the X-components of the force vectors have opposite signs on the left and right sides, reflecting their mirrored orientation relative to the sagittal (YZ) plane. However, the magnitudes of the applied muscle forces differ between the working and balancing sides due to the side-dependent activation scaling factors. Thus, the applied loading is asymmetric in magnitude rather than in the definition of the force

directions. Figure 6 illustrates the spatial arrangement of the applied muscle forces and boundary conditions.

**Table 2.** Muscle force vectors applied to simulate functional loading [38,48,49].

| Muscle Group | RF, N | 60% RF, N | Scaling Factor | | Unit Vector Coordinates | | | Right Force Components, N | | | Left Force Components, N | | |
|---|---|---|---|---|---|---|---|---|---|---|---|---|---|
| | | | R (BS) | L (WS) | X | Y | Z | X | Y | Z | X | Y | Z |
| Superficial masseter | 190.40 | 114.24 | 0.60 | 0.72 | −0.207 | 0.885 | 0.419 | −14.2 | 60.7 | 28.7 | 17.0 | 72.8 | 34.5 |
| Deep masseter | 81.60 | 48.96 | 0.60 | 0.72 | −0.546 | 0.758 | −0.358 | −16.0 | 22.3 | −10.5 | 19.2 | 26.7 | −12.6 |
| Medial pterygoid | 174.80 | 104.88 | 0.60 | 0.84 | 0.486 | 0.791 | 0.372 | 30.6 | 49.8 | 23.4 | −42.8 | 69.7 | 32.8 |
| Anterior temporalis | 158.00 | 94.80 | 0.58 | 0.73 | −0.149 | 0.988 | 0.044 | −8.2 | 54.3 | 2.4 | 10.3 | 68.4 | 3.0 |
| Middle temporalis | 95.60 | 57.36 | 0.67 | 0.66 | −0.221 | 0.837 | −0.5 | −8.5 | 32.2 | −19.2 | 8.4 | 31.7 | −18.9 |
| Posterior temporalis | 75.60 | 45.36 | 0.39 | 0.59 | −0.208 | 0.474 | −0.855 | −3.7 | 8.4 | −15.1 | 5.6 | 12.7 | −22.9 |
| Inferior lateral pterygoid | 66.90 | 40.14 | 0.65 | 0.30 | 0.63 | −0.174 | 0.757 | 16.4 | −4.5 | 19.8 | −7.6 | −2.1 | 9.1 |

RF—Reduced Force; R (BS)—Right (Balancing Side); L (WS)—Left (Working Side).

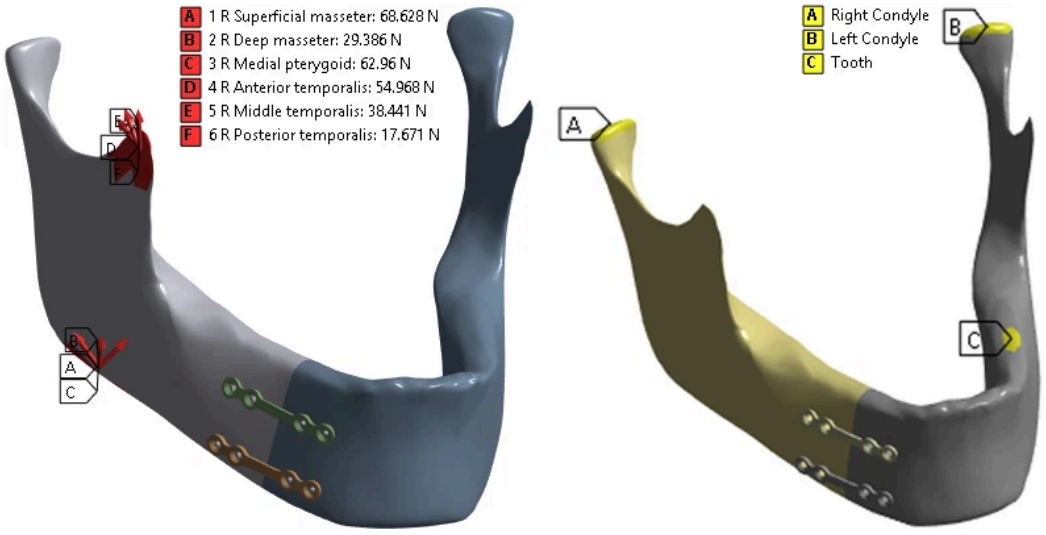


**Figure 6.** Applied muscle loading and boundary conditions.

The condyles were modeled as stationary supports, while the molar was vertically immobilized to simulate occlusal contact (Figure 6).

To enhance simulation accuracy, the effects of screw tightening were incorporated, generating tensile stresses in the screws and compressive stresses in the mandible and miniplates.

The stress–strain state of the restored mandible was analyzed in two stages: pretension loads were applied to individual screws, and muscle forces were introduced in the second phase.

A submodeling approach was utilized for a more detailed analysis of the fracture fixation site. A high-resolution finite element mesh was applied to the submodel to improve computational accuracy (Figure 7).

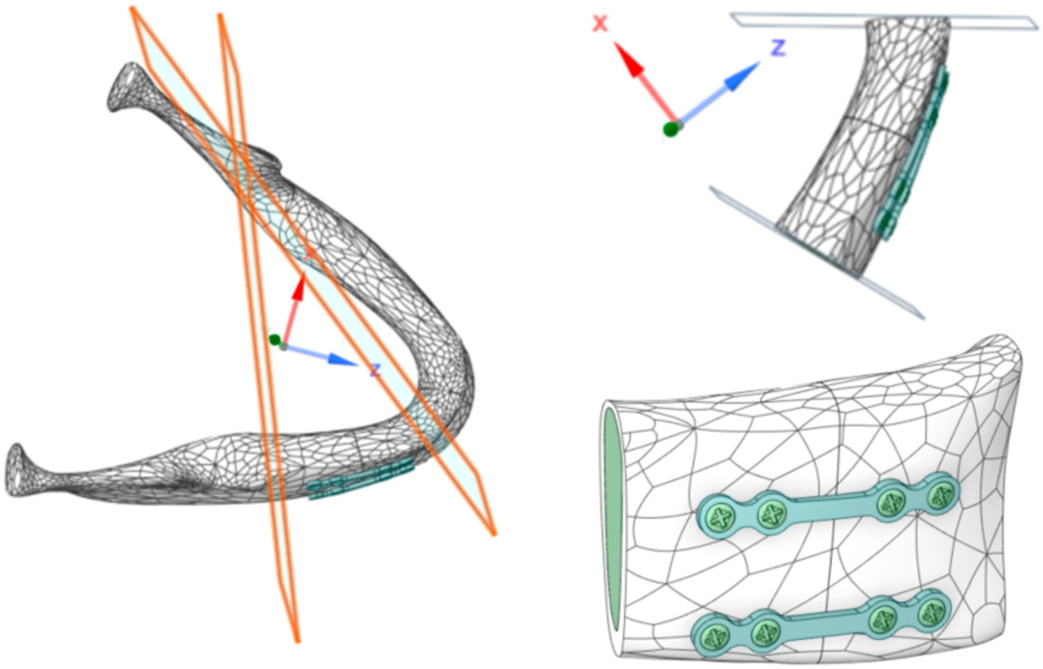


**Figure 7.** Extraction of the submodel from the global mandibular model. The orange rectangles represent the cutting planes defining the boundaries of the submodel.

Finite element analysis was conducted using the following element types: SOLID185—3D solid structure modelling; SOLID285—low-order 3D tetrahedral element; CONTA174—contact and sliding representation; TARGE170—3D target surface modelling; BEAM188—structural beam analysis; PRETS179—pretension element for structural preloading.

A separate mesh refinement study was performed using the global mandibular finite element representation to evaluate the sensitivity of the structural response to discretization size. Six meshes with nominal element sizes ranging from 1.8 to 0.4 mm were investigated. The total strain energy and maximum displacement were selected as convergence indicators. The number of mesh nodes, the corresponding number of algebraic unknowns, and the convergence results are reported in Table 3. The finest discretization was used as the reference for calculating relative differences.

**Table 3.** Convergence of energy and maximum displacement with mesh refinement.

| Element Size | Number of | | Computation Time * | Energy | | Displacement | |
|---|---|---|---|---|---|---|---|
| | Nodes | Unknowns | | Value, mJ | Err, % | Value, mm | Err, % |
| 1.8 | 220,241 | 661,225 | 36 m 11 s | 47.26 | 7.29 | 0.745 | 2.34 |
| 1.5 | 378,517 | 1,136,123 | 55 m 16 s | 46.07 | 4.59 | 0.737 | 1.28 |
| 1.0 | 1,191,231 | 3,574,265 | 1 h 2 m | 45.50 | 3.29 | 0.735 | 0.96 |
| 0.8 | 1,536,149 | 4,609,019 | 1 h 50 m | 45.20 | 2.61 | 0.733 | 0.69 |
| 0.6 | 2,871,585 | 8,615,327 | 2 h 12 m | 44.75 | 1.59 | 0.730 | 0.27 |
| 0.4 | 6,809,122 | 20,427,938 | 3 h 51 m | 44.05 | – | 0.728 | – |

* The computation time was measured using 24 Intel® Xeon® Gold 6415H processors (2.10 GHz) with 256 GB of RAM.

The mesh convergence results demonstrate a progressive stabilization of the calculated displacement and strain energy with increasing mesh resolution. Refining the element size from 1.0 to 0.6 mm increased the number of unknowns by approximately 2.4 times, while the maximum displacement and strain energy changed by approximately 0.7% and 1.7%, respectively. Further refinement from 0.6 to 0.4 mm resulted in differences of approximately

0.27% in maximum displacement and 1.59% in strain energy, relative to the finest mesh. These results indicate satisfactory convergence of the investigated global response quantities [50,51]. Accordingly, the mesh with an average element size of 0.4 mm was selected for the final analysis (Figure 8).

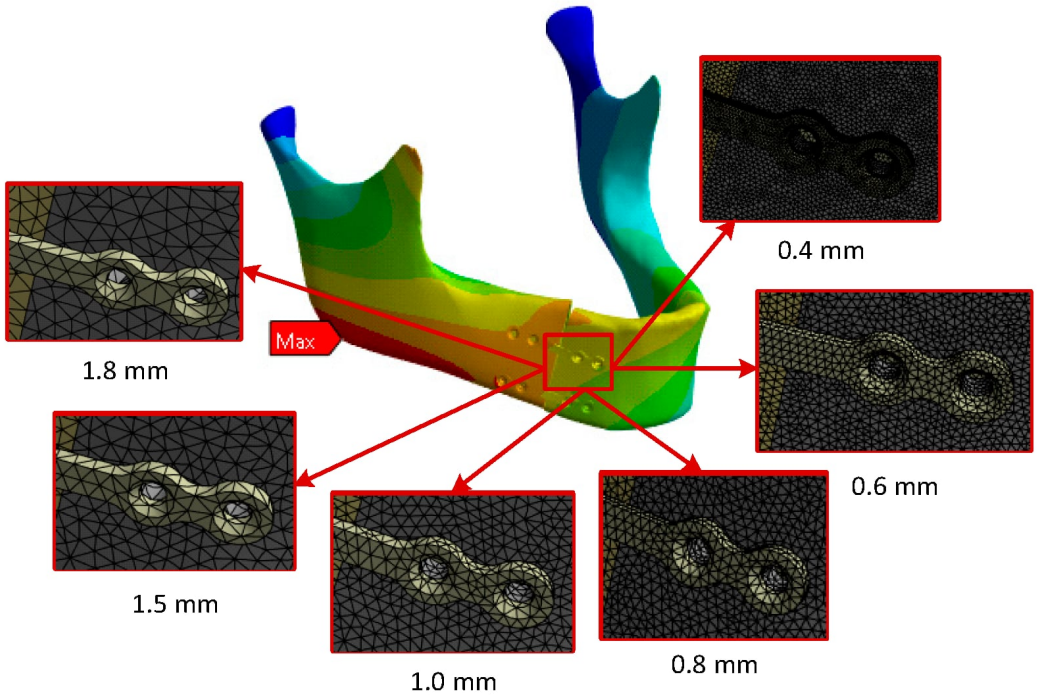


**Figure 8.** Finite element mesh in local zones.

For submodel calculations, the average finite element mesh size was set to 0.4 mm for cortical bone, 0.2 mm for screws and plates, and 0.8 mm for cancellous bone. The element size on hole surfaces was reduced to 0.1 mm (Figure 9).

Table 4 presents the finite element mesh statistics for the global mandibular models and the corresponding locally refined submodels of both fixation configurations. The reported total element counts include structural solid elements (SOLID185 and SOLID285), whereas contact, target, beam, and pretension elements are excluded. The differences in mesh statistics reflect the distinct geometric representations and discretization strategies adopted for the global models and submodels.

**Table 4.** Finite element mesh statistics of the global mandibular models and locally refined submodels for both miniplate configurations.

| Number of Finite Elements/Nodes | Model with Miniplate 27 × 2.5 × 1.25 | | Model with Miniplate 20.5 × 3.5 × 1.25 | |
|---|---|---|---|---|
| **Component** | **Global Model** | **Submodel** | **Global Model** | **Submodel** |
| Cortical bone | 592,062/127,575 | 7,967,478/1,449,287 | 576,523/882,479 | 6,019,726/1,092,324 |
| Cancellous bone | 488,838/94,140 | 2,485,814/443,387 | 304,625/446,146 | 585,491/108,543 |
| Miniplates | 15,576/20,586 | 316,587/352,552 | 13,902/68,445 | 270,356/302,260 |
| Screws | 16/24 | 2,306,982/491,153 | 16/24 | 2,309,188/491,538 |
| Total | 1,096,476/233,532 | 13,076,849/2,694,630 | 895,050/1,397,070 | 9,184,759/1,988,269 |

Note: Element counts in the Total row refer to SOLID185 and SOLID285 elements. The global-model screw entries represent BEAM188 elements and are excluded from these totals. Nodal totals represent model-level node counts and are not calculated by summing the component-wise values.

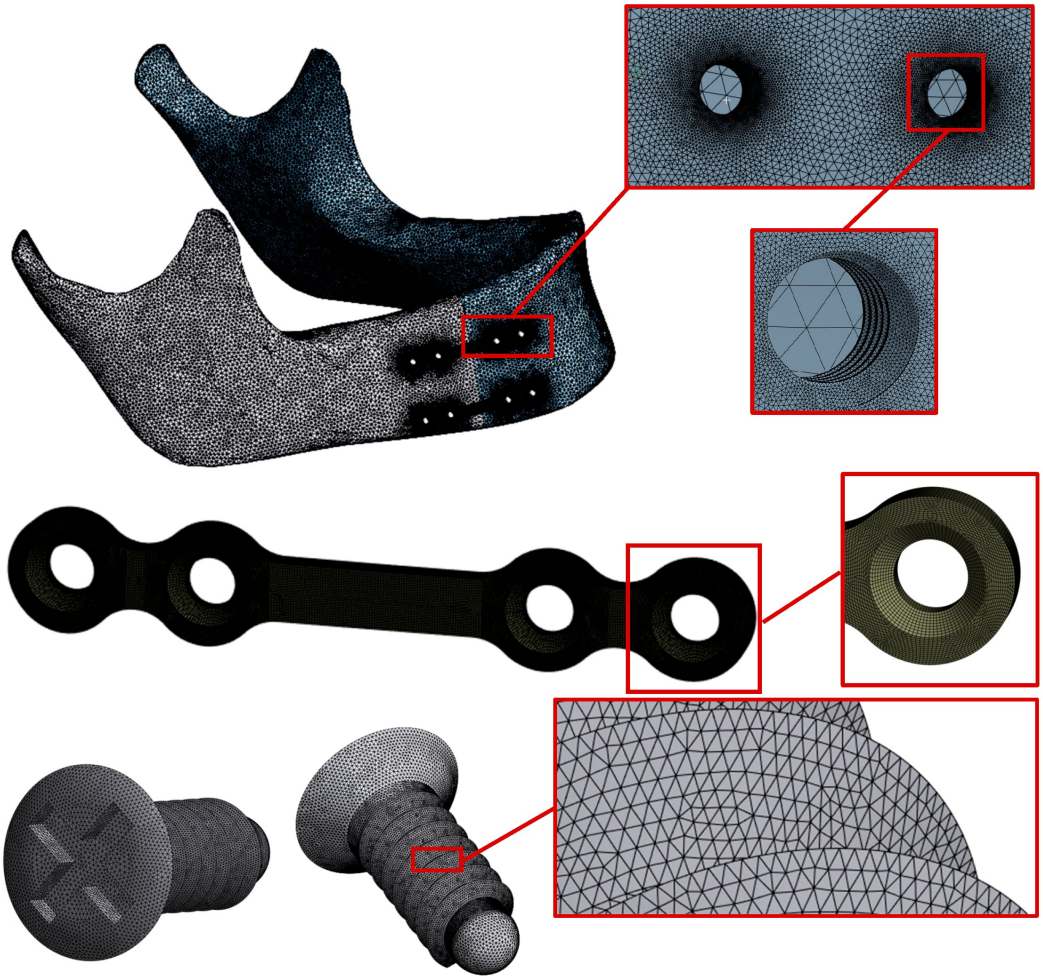

**Figure 9.** Finite element mesh in different local zones.

The contact problem under consideration exhibits significant nonlinearity, requiring modifications to the system stiffness matrix to account for individual component interactions at different contact levels. Contact determination is initiated when the contact and target surfaces come into contact.

## 3. Results

The numerical analysis demonstrated that different miniplate configurations resulted in varying force distributions across the mandible (Figure 10).

Although the overall applied force remained constant, the distribution of reaction forces at the mandibular condyles and the first molar differed slightly between the two miniplate configurations. These differences indicate that plate geometry influences load transfer within the mandibular fixation system.

Evaluations included the displacement distribution (Figure 11), cortical bone gap (Figure 12), and sliding distance across the fracture section (Figure 13).

The findings indicate that miniplate dimensions play a significant role in the biomechanical stability of mandibular fracture fixation. The 27 × 2.5 × 1.25 mm miniplate exhibited greater displacement (0.728 mm) compared to the 20.5 × 3.5 × 1.25 mm miniplate (0.628 mm), suggesting that the narrower plate allows for more flexibility under load. While increased flexibility may facilitate adaptation to dynamic forces, it could also lead to higher stress concentrations at fixation points.

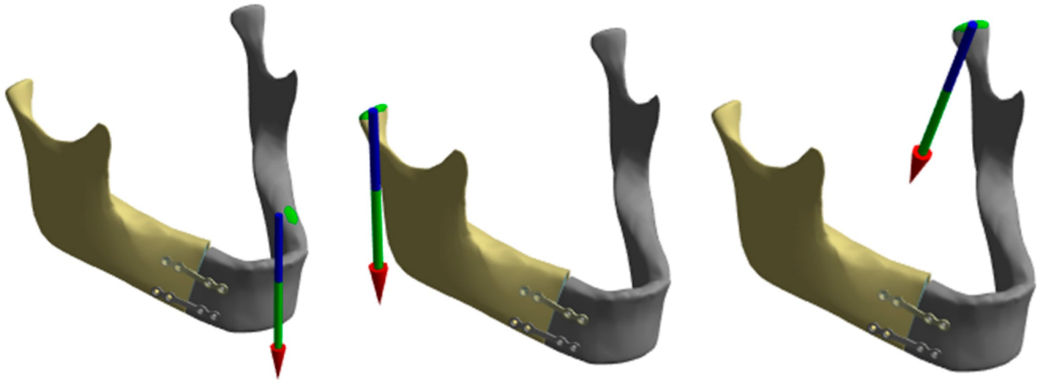

| | | | |
|---|---|---|---|
| miniplate 27 × 2.5 × 1.25 | 308 N | 142 N | 65 N |
| miniplate 20.5 × 3.5 × 1.25 | 308 N | 143 N | 63 N |

**Figure 10.** Magnitudes of the resultant reaction forces at the left and right mandibular condyles and the first molar for the two investigated miniplate configurations.

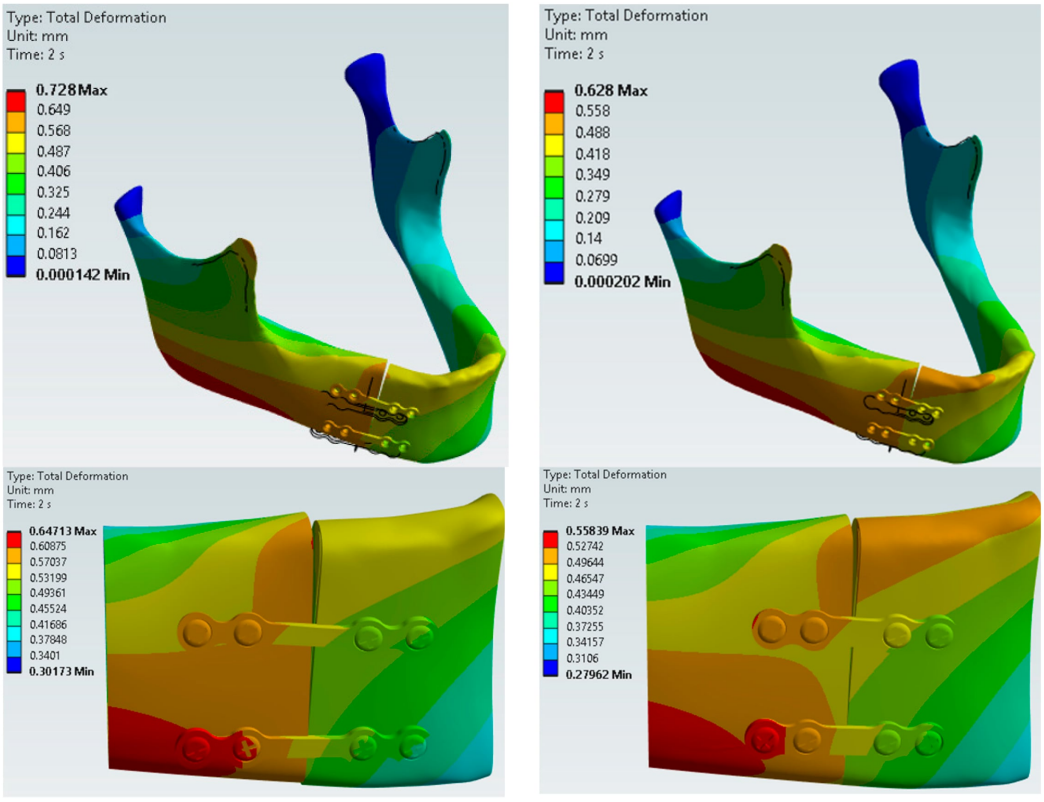


miniplate 27 × 2.5 × 1.25 miniplate 20.5 × 3.5 × 1.25

**Figure 11.** Resulting displacement distribution plot (×20).

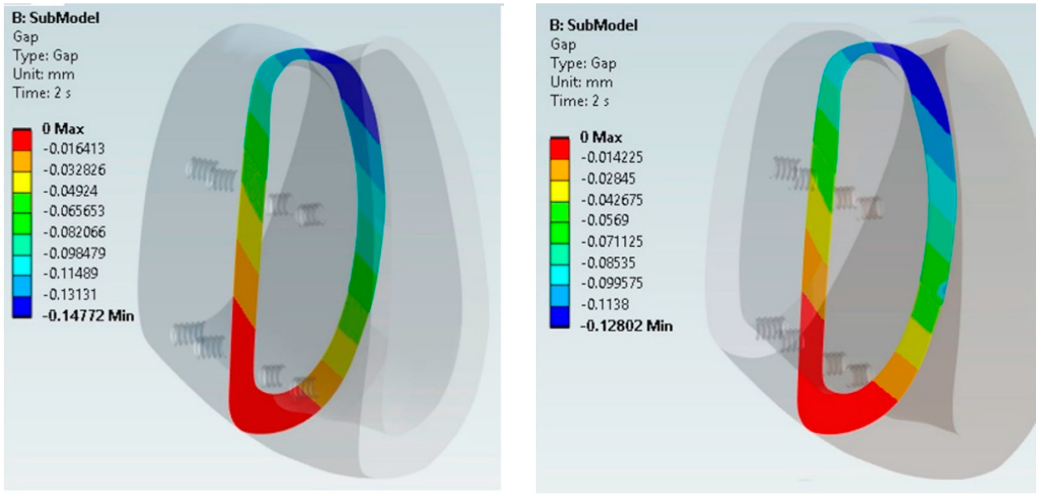


miniplate 27 × 2.5 × 1.25 miniplate 20.5 × 3.5 × 1.25

**Figure 12.** Fracture gap distribution at the cortical bone interface (negative values indicate opening) (×20).

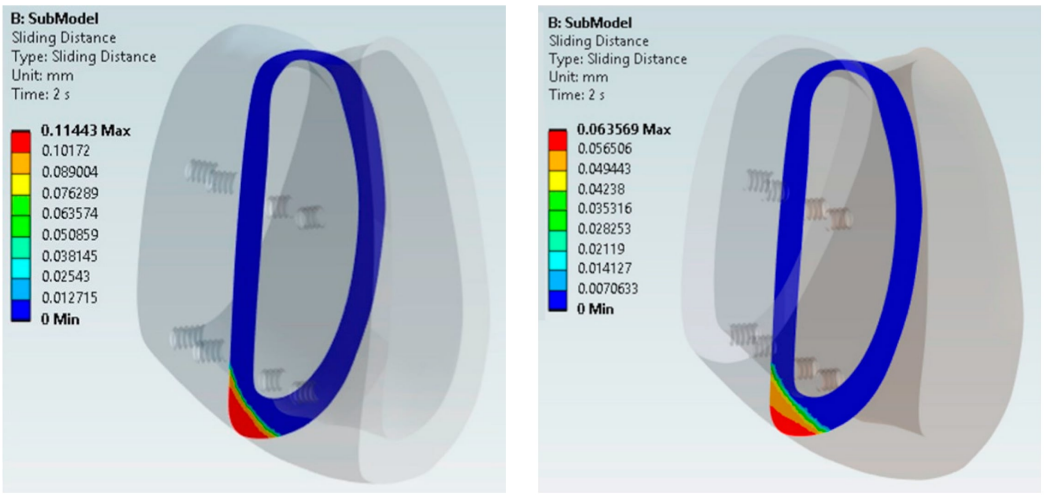


miniplate 27 × 2.5 × 1.25 miniplate 20.5 × 3.5 × 1.25

**Figure 13.** Cortical bone sliding distance in the fracture section (×20).

The fracture exhibited nonuniform deformation under the applied loading conditions, with opening in the superior cortical region and localized contact between the inferior cortical surfaces. The maximum fracture opening was slightly larger for the 27 × 2.5 × 1.25 mm miniplate (0.15 mm) than for the 20.5 × 3.5 × 1.25 mm miniplate (0.13 mm). The negative gap values in Figure 12 indicate separation of the fracture surfaces, with their absolute magnitudes representing the corresponding opening. The inferior cortical regions transmitted compressive and tangential forces, as confirmed by the contact pressure and frictional stress distributions . The absolute difference of 0.02 mm indicates a relatively small effect of plate geometry on fracture opening under the investigated loading conditions. However, the clinical significance of these predicted displacements cannot be established from the present finite element analysis alone.

The relative cortical bone sliding distance was measured at 0.11 mm for the 27 × 2.5 × 1.25 mm miniplate and 0.06 mm for the 20.5 × 3.5 × 1.25 mm miniplate, confirming that the wider plate provides better restriction of movement at the fracture site. This enhanced stabilization indicates improved mechanical control of interfragmentary motion under the investigated loading conditions.

To assess the mechanical significance of the predicted interfragmentary displacements, the maximum normal opening and tangential sliding were considered separately and normalized by the assumed initial fracture gap of 0.5 mm. The resulting nominal opening-to-gap ratios were 30% and 26% for the narrower and wider miniplate configurations, respectively. The corresponding shear-displacement-to-gap ratios were 22% and 12%. These quantities provide a comparative description of the relative motion between the fracture fragments but do not represent local strains within the healing tissue. In particular, the maximum opening and sliding displacements may occur at different locations along the fracture interface. According to the interfragmentary strain concept proposed by Perren [52], the mechanical conditions for fracture healing depend on the deformation relative to the fracture gap and the tolerance of the developing repair tissue. Consequently, the calculated displacements should not be interpreted using a universal absolute micromotion threshold. The lower opening and sliding values obtained for the wider miniplate indicate improved mechanical stabilization, although the implications for fracture healing cannot be established without a more detailed representation of the fracture gap and healing tissues.

Overall, the results suggest that plate geometry plays a crucial role in optimizing fracture fixation. Wider plates offer improved stability and reduced cortical bone movement, while narrower plates provide greater flexibility, which may be beneficial in some cases. Selecting the optimal fixation approach requires balancing rigidity and adaptability based on patient-specific conditions.

The stress distribution patterns in both analyzed cases are similar (Figure 14). Stress peaks are observed at the bone contact area and near the upper plate fixation holes. These locations are responsible for transmitting bending moments caused by tensile forces in the upper plate and compressive forces at the contact point.

The 27 × 2.5 × 1.25 mm miniplate generated a frictional stress of 8.1 MPa, whereas the 20.5 × 3.5 × 1.25 mm miniplate produced 6.3 MPa (Figure 15). Higher frictional stress in the narrower plate may contribute to increased resistance against micromovements but could also result in higher localized wear at the bone–bone interface.

The pressure distribution at the fracture interface was 26.9 MPa for the 27 × 2.5 × 1.25 mm miniplate and 21.1 MPa for the 20.5 × 3.5 × 1.25 mm miniplate (Figure 16). The differences in fracture-interface contact pressure reflect the redistribution of contact forces between the bone fragments under the prescribed loading conditions and should not be interpreted as evidence of stress shielding.

The maximum von Mises stress in the miniplates reached 341 MPa for the 27 × 2.5 × 1.25 mm configuration and 287 MPa for the 20.5 × 3.5 × 1.25 mm configuration (Figure 17), corresponding to a reduction of approximately 15.8% for the shorter, wider miniplates. In both configurations, the superior plate exhibited more pronounced stress concentrations, particularly near the fixation holes. This behaviour is associated with the combined effects of tensile loading induced by mandibular bending and shear loading associated with torsion at the fracture site. The lower peak stress in the shorter, wider configuration indicates a more favourable stress response under the investigated loading conditions.

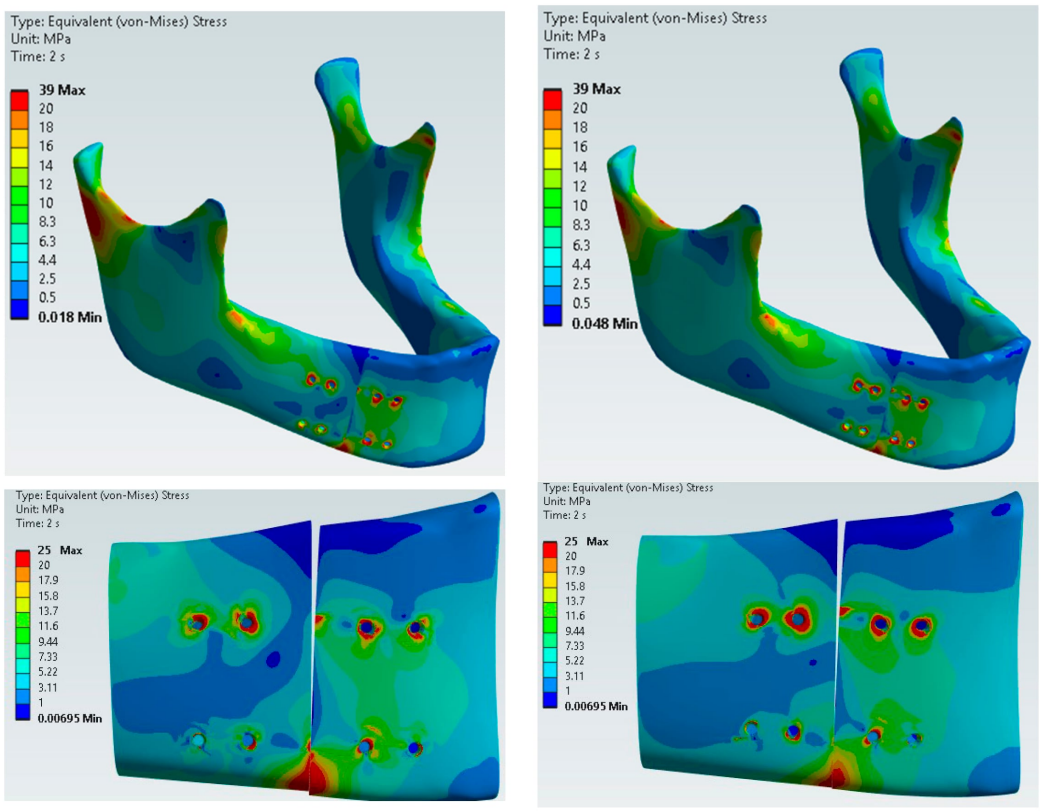


miniplate 27 × 2.5 × 1.25 miniplate 20.5 × 3.5 × 1.25

**Figure 14.** Stress distribution (von Mises equivalent stress) in the bone after screw tightening and subsequent muscle force loading (×20).

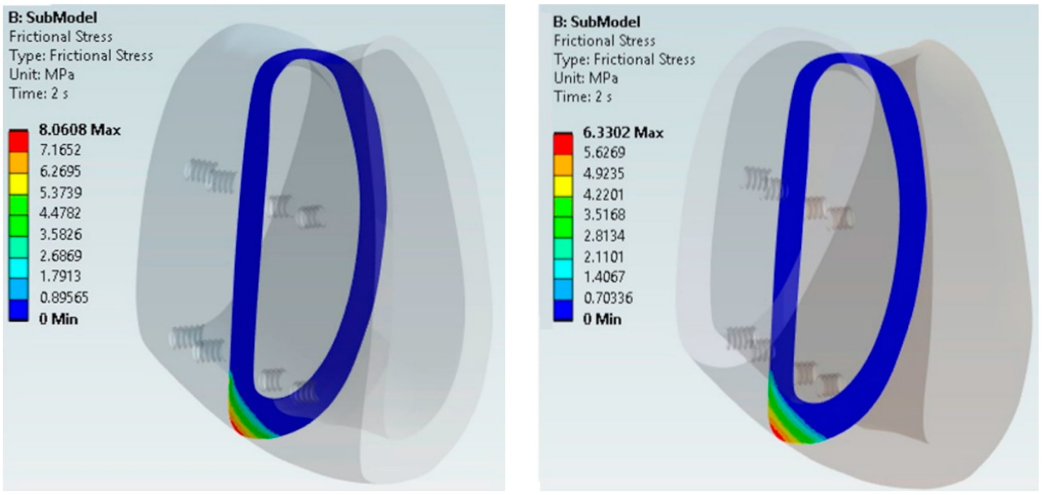


miniplate 27 × 2.5 × 1.25 miniplate 20.5 × 3.5 × 1.25

**Figure 15.** Frictional stress distribution in the cortical bone at the fracture section (×20).

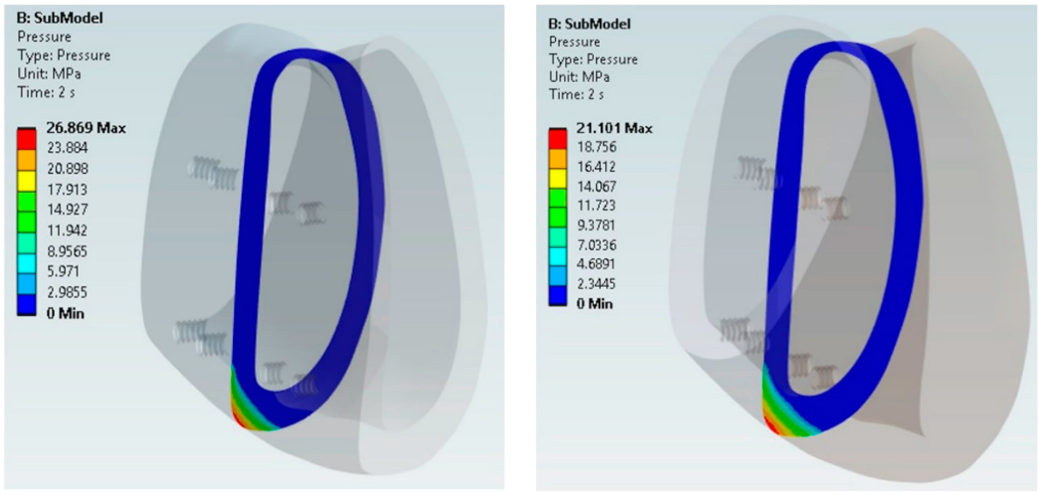


miniplate 27 × 2.5 × 1.25 miniplate 20.5 × 3.5 × 1.25

**Figure 16.** Cortical bone pressure distribution in the fracture section (×20).

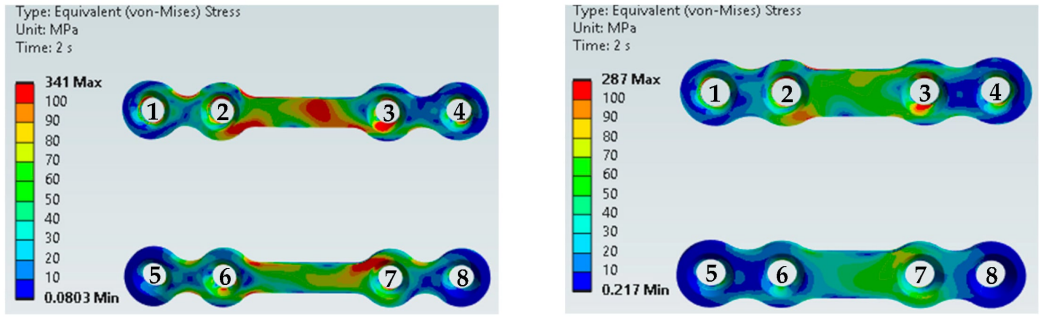


miniplate 27 × 2.5 × 1.25 miniplate 20.5 × 3.5 × 1.25

**Figure 17.** Stress distribution (von Mises equivalent stress) in the miniplates: 1–8 screw numbers.

The screw stress distributions exhibit localized concentrations, particularly near the screw heads and the plate–screw interfaces (Figure 18).

The upper fixation assembly generally experiences greater loading, consistent with the transfer of bending and torsional moments across the fracture. Elevated stresses are also observed in screws No. 2 and No. 7, which are subjected to pronounced axial loading. Despite these local concentrations, the overall maximum von Mises stresses are comparable between the two configurations, reaching 250 MPa and 220 MPa for the longer, narrower and shorter, wider miniplates, respectively.

The principal biomechanical outcomes for both miniplate configurations, together with their absolute and relative differences, are summarized in Table 5. Compared with the longer, narrower configuration, the shorter, wider miniplate reduced maximum mandibular displacement by 13.7%, fracture opening by 13.3%, interfragmentary sliding by 45.5%, and maximum von Mises stresses in the plates and screws by 15.8% and 12.0%, respectively. These differences characterize the predicted comparative mechanical response under the prescribed static loading and contact conditions; their sensitivity to variations in screw pretension, interface friction, and local mesh refinement remains to be established.

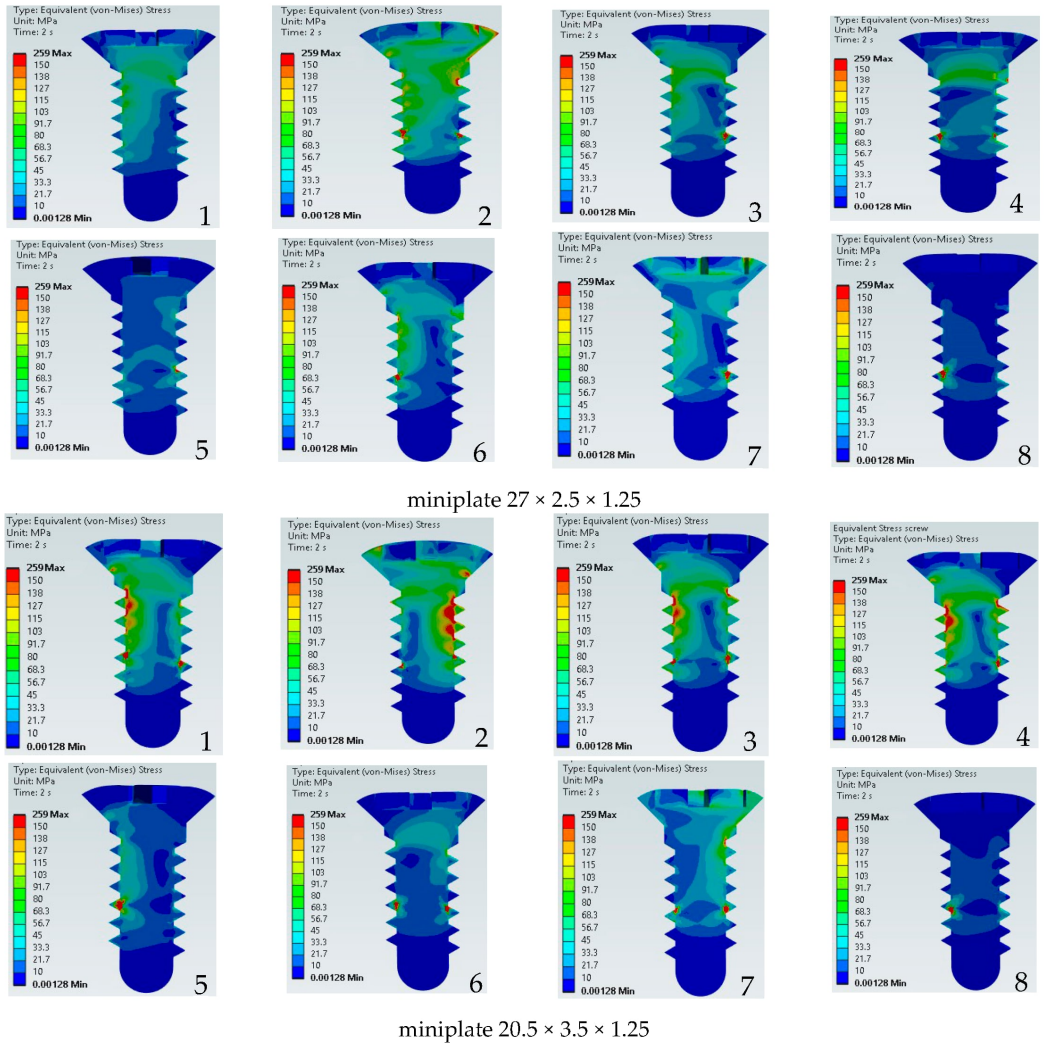


**Figure 18.** Stress distribution (von Mises equivalent stress) in screws. A common colour scale is used to facilitate direct comparison of the stress distributions.

**Table 5.** Comparison of the principal biomechanical results for the two miniplate configurations.

| Biomechanical Parameter | 27 × 2.5 × 1.25 mm | 20.5 × 3.5 × 1.25 mm | Difference | |
|---|---|---|---|---|
| | | | Absolute | Relative |
| Reported maximum mandibular displacement, mm | 0.728 | 0.628 | −0.1 | −13.7% |
| Cortical bone gap, mm | 0.15 | 0.13 | −0.02 | −13.3% |
| Interfragmentary sliding distance, mm | 0.11 | 0.06 | −0.05 | −45.5% |
| Maximum frictional stress at the fracture interface, MPa | 8.1 | 6.3 | −1.8 | −22.2% |
| Maximum contact pressure at the fracture interface, MPa | 26.9 | 21.1 | −5.8 | −21.6% |
| Maximum von Mises stress in miniplates, MPa | 341 | 287 | −54 | −15.8% |
| Reported maximum von Mises stress in screws, MPa | 250 | 220 | −30 | −12.0% |
| First molar reaction force, | 308 | 308 | 0 | 0 |
| Condylar reaction force 1, | 65 | 63 | −2 | −3.1% |
| Condylar reaction force 2, N | 142 | 143 | +1 | +0.7% |

Note: Absolute and relative differences were calculated using the longer, narrower miniplate (27 × 2.5 × 1.25 mm) as the reference configuration. Negative values indicate a reduction in the corresponding parameter for the shorter, wider miniplate (20.5 × 3.5 × 1.25 mm). The reported fracture opening represents the maximum normal separation obtained from the contact analysis under loading, rather than the prescribed initial geometric fracture gap of approximately 0.5 mm.

The present results demonstrate differences in the mechanical response of the two investigated miniplate configurations under the prescribed static loading conditions. The shorter, wider miniplate exhibited lower interfragmentary displacements and reduced stress concentrations in the fixation components. However, these findings should not be interpreted as evidence of improved fracture healing or clinical superiority, since biological healing processes and long-term clinical outcomes were not evaluated.

Figure 19 presents a clinical example of mandibular fracture fixation using osteosynthesis miniplates. This radiographic illustration provides clinical context but does not constitute experimental validation of the numerical results or establish the comparative effectiveness of the investigated configurations.

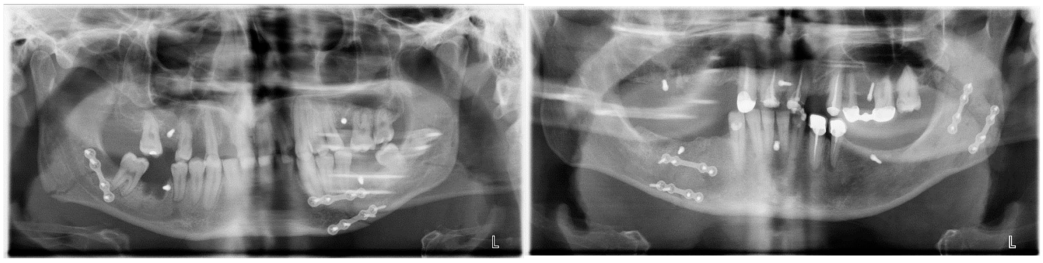

**Figure 19.** Radiographic assessment of miniplate fixation in a patient with mandibular fracture.

## 4. Discussion

This study provides an in-depth analysis of the biomechanical behavior of mandibular fracture fixation using finite element modeling. The findings emphasize the critical role of miniplate dimensions in determining stress distribution, displacement, and overall stabilization during the healing process.

A key observation is that miniplate design significantly influences the mechanical stability of the fracture site. The comparison between the two miniplate configurations (27 × 2.5 × 1.25 mm and 20.5 × 3.5 × 1.25 mm) revealed that the wider, shorter plate resulted in lower displacement and reduced cortical bone movement under the investigated loading conditions. These findings are consistent with previous finite element studies demonstrating that fixation plate geometry, configuration, and positioning influence stress distribution and interfragmentary stability in mandibular osteosynthesis [30,31,33,36]. However, since the investigated configurations differ in both plate length and width, as well as potentially in screw positioning, the observed differences in biomechanical response cannot be attributed to plate width alone. The present results therefore characterize the combined mechanical effects of the two fixation configurations rather than the isolated influence of individual geometric parameters.

The mechanical environment of mandibular fracture healing should be evaluated in terms of interfragmentary strain rather than an absolute displacement threshold. According to Perren's interfragmentary strain theory [52], the biological response of the healing tissue depends on its deformation relative to the initial fracture gap. In the present study, the predicted normal opening (0.15 and 0.13 mm) and tangential sliding (0.11 and 0.06 mm) correspond to nominal displacement-to-gap ratios of 26–30% and 12–22%, respectively, considering the assumed initial gap of 0.5 mm. These relatively high ratios indicate substantial interfragmentary motion and should not be interpreted as evidence of mechanically favorable conditions for fracture healing. Moreover, normal opening and tangential sliding represent different deformation modes and may affect the healing tissue differently. Since the present model does not explicitly incorporate fracture callus or evolving tissue properties, the calculated ratios cannot be directly equated with local tissue strains or used to predict healing outcomes. Nevertheless, the shorter, wider miniplate demonstrated lower

opening and sliding displacements, indicating improved mechanical stabilization under the investigated loading conditions.

The simulated reaction force at the first molar was 308 N under the prescribed postoperative muscle loading conditions. Although previously reported maximum molar bite forces in healthy adults are approximately 506 N [53,54], this comparison cannot be considered an independent validation of the finite element model, since the predicted reaction force is determined by muscle forces and activation assumptions derived from the literature. Furthermore, the reference muscle forces were reduced to 60% of their original magnitudes, with additional muscle-specific and side-dependent scaling factors applied as specified in Table 2. Therefore, directly extrapolating the calculated reaction force of 308 N to an equivalent maximum bite force of 513 N by dividing by 0.60 would neglect the effects of these additional scaling factors. The predicted reaction force should instead be interpreted as a model-dependent response under the prescribed loading scenario. Experimental measurements of postoperative bite forces or mandibular deformation would be required for independent quantitative validation of the model.

Stress distribution analysis indicated that the superior miniplate was predominantly subjected to tensile loading, whereas the inferior plate experienced mainly compressive loading. This pattern is consistent with the biomechanical principles underlying Champy's osteosynthesis approach. The predicted stress distributions also revealed differences in load transfer between the investigated fixation configurations under the prescribed static loading conditions.

The maximum von Mises stresses in the fixation screws were approximately 250 MPa for the longer, narrower configuration and 220 MPa for the shorter, wider configuration. These values characterize the local mechanical response under the assumed loading, contact, and pretension conditions. However, they do not establish differences in screw loosening, fatigue resistance, or long-term fixation durability, since cyclic loading, progressive interface degradation, and fatigue damage were not investigated.

The representation of screw pretension and threaded screw–bone interaction is an important consideration in the biomechanical assessment of mandibular fracture fixation systems [55]. The mechanical response of the screw–bone interface depends on the thread geometry, local bone properties, and contact conditions, which may substantially influence the predicted stress distribution in the surrounding bone [55]. Furthermore, the initial screw preload is closely related to the mechanical engagement of the threaded fixation system and its resistance to axial pull-out [56]. In the present study, the screw pretension was determined from an auxiliary finite element pull-out analysis explicitly accounting for the screw threads and their interaction with cortical bone. The resulting pretension was subsequently applied to equivalent screw connections in the global mandibular model, while a refined three-dimensional submodel was used to evaluate local stress distributions around the threaded interfaces. This multilevel modelling approach provided a consistent mechanical basis for comparing the two miniplate configurations under identical initial fixation conditions. Nevertheless, the selected pretension should be regarded as a model-specific numerical estimate rather than an experimentally validated optimal tightening force, since its magnitude depends on the assumed bone properties, screw geometry, and interface conditions.

Interfragmentary opening and sliding were also evaluated to characterize the relative mechanical stability of the fixation configurations. The shorter, wider configuration exhibited lower predicted interfragmentary displacements under the investigated static loading conditions. Although reduced relative motion may be relevant to the mechanical environment at the fracture site, the present model does not include healing tissue evolution

or biological repair mechanisms. Therefore, these results cannot be directly interpreted as evidence of improved fracture healing.

The prescribed postoperative muscle loading produced different reaction force and stress distributions for the two configurations. These differences provide insight into their comparative mechanical behaviour but do not establish their clinical effectiveness or suitability for individual patients.

The observed differences in mechanical response reflect the combined influence of the geometric characteristics of the investigated miniplate configurations. The shorter and wider miniplate (20.5 × 3.5 × 1.25 mm) exhibited lower interfragmentary displacement and reduced stress concentrations compared with the longer and narrower configuration (27 × 2.5 × 1.25 mm). However, since the configurations differ simultaneously in length and width, and potentially in screw positioning, these differences cannot be attributed to a single geometric parameter. The results therefore demonstrate the comparative mechanical performance of the selected fixation configurations rather than establishing an independent effect of plate width or surface area.

Under the investigated static loading conditions, the shorter, wider miniplate configuration (20.5 × 3.5 × 1.25 mm) exhibited lower maximum plate stresses and reduced interfragmentary motion compared with the longer, narrower configuration (27 × 2.5 × 1.25 mm). However, because the two configurations differ in both length and width, and potentially in screw positioning, these differences cannot be attributed to plate width alone. The results provide a comparative assessment of the mechanical behaviour of the two investigated fixation configurations but do not establish superior clinical performance, improved fracture healing, or reduced fatigue-related failure risk.

Future research should focus on assessing the long-term effects of different fixation systems, particularly their influence on bone remodeling and fixation devices' longevity.

Previous numerical and experimental investigations have demonstrated that the mechanical stability of mandibular fracture fixation depends on the type, configuration, and positioning of osteosynthesis plates [31,33,34]. Building on these findings, the present study focuses on the influence of miniplate dimensions on the stress–strain response of the fixation system under identical loading and boundary conditions. To investigate these effects, the finite element modelling approach incorporated the following:

- Distinct material properties of cortical and cancellous bone to accurately capture their biomechanical behavior.
- Realistic cortical bone thickness to improve the precision of mechanical response predictions.
- Contact interactions at the bone-fixation device interface to simulate realistic fixation mechanics.
- Detailed screw thread geometry to enhance the accuracy of force transmission modeling.

The incorporation of these modelling features enabled a more detailed assessment of local stress distributions, interfragmentary displacements, and screw–bone interactions. However, the predictive accuracy of the model and its applicability to clinical conditions require further experimental validation.

The present finite element model incorporates muscle loading, screw pretension, and frictional contact to compare the mechanical response of two mandibular fracture fixation configurations. Under the prescribed static loading conditions, both configurations provided mechanical stabilization, while differences were observed in plate stresses and interfragmentary displacements. However, the present analysis does not independently evaluate stress shielding, long-term implant performance, or clinical outcomes. There-

fore, the results should not be interpreted as establishing the clinical superiority of either configuration or as providing general recommendations for plate selection.

Despite its strengths, this study has certain limitations. The assumption of linear elastic isotropic behaviour for cortical and cancellous bone simplifies the numerical analysis but does not fully capture the direction-dependent, time-dependent, and nonlinear mechanical response of bone tissue [57]. Previous studies have demonstrated the influence of cortical bone orthotropy on mandibular strain predictions [58]. More recently, the authors of [59] investigated an orthotropic visco-plasto-damage constitutive model and demonstrated its applicability to bone structures, including the mandible. Although the simplified material description adopted in the present study provides a consistent basis for comparing the two miniplate configurations, it does not account for irreversible deformation or progressive bone damage.

The friction coefficient of 0.3 was assumed to be constant at the bone–bone and bone–plate interfaces. Although this value is consistent with previously published finite element modelling assumptions [34], it was not determined experimentally for the present mandibular fixation system. Moreover, other studies have adopted different interface formulations, including no-slip conditions [33] and frictionless or bonded contacts [31]. Therefore, the predicted contact pressures, frictional stresses, and interfragmentary sliding may depend on the selected contact parameters. A sensitivity analysis of these parameters would be valuable in future investigations.

The sensitivity of the predicted biomechanical response to screw pretension, postoperative muscle activation, and condylar boundary conditions was not systematically investigated. Although the screw pretension of 130 N was derived from a separate finite element analysis of the threaded screw–bone interface, this procedure establishes a mechanically motivated reference value rather than demonstrating insensitivity to preload variations. In particular, changes in screw pretension may modify the normal contact pressure between the plate and bone and thereby influence frictional resistance, load transfer, and local stress concentrations. These effects may interact with the assumed fracture-interface friction and affect the relative displacement of the bone fragments. Although identical modelling assumptions were applied to both fixation configurations, the stability of their comparative ranking under alternative parameter combinations has not been established. A targeted sensitivity analysis of screw pretension and interface friction, followed by assessment of interfragmentary opening, sliding, and fixation stresses, is therefore required to quantify the robustness of the comparative findings. Such additional nonlinear contact simulations remain a priority for future investigations.

Anatomical consideration concerns the positioning of the superior miniplate, which was placed 4 mm below the alveolar crest in the present model. Although superior miniplate fixation is consistent with established mandibular osteosynthesis principles, this distance does not necessarily ensure adequate clearance from the dental roots. The risk of root interference depends on individual dental anatomy, screw length, insertion direction, and the location of the plate holes. Therefore, the investigated plate position should be regarded as a standardized modelling assumption rather than a universally applicable surgical recommendation. In clinical practice, plate and screw placement must be adapted to the patient-specific anatomy to avoid damage to the dental roots.

An additional limitation is the absence of independent experimental validation of the predicted mandibular reaction forces, interfragmentary displacements, and fixation stresses. The muscle forces and their activation factors were adopted from published studies rather than obtained from patient-specific measurements. Consequently, agreement between the calculated molar reaction force and the literature-reported bite forces cannot establish predictive accuracy, since these quantities are not independent of the prescribed loading as-

sumptions. Future studies should validate the model against experimentally measured bite forces, interfragmentary micromotions, or strain measurements under controlled loading conditions.

Although the mesh refinement study indicated stabilization of the global strain energy and maximum displacement, convergence of the local interfragmentary opening, sliding, and peak screw stresses was not independently established. These quantities may exhibit greater sensitivity to local discretization, particularly in the vicinity of contact interfaces and geometric discontinuities. An extended convergence analysis involving the nonlinear contact submodels was beyond the computational resources currently available. Consequently, the reported local mechanical responses should be interpreted as comparative numerical predictions under the adopted modelling assumptions, while their quantitative mesh sensitivity remains to be established.

While finite element analysis provides valuable insights, it cannot entirely replicate in vivo conditions. Variability in patient-specific bone density was not explicitly modelled, which may affect stress distribution in clinical cases. Furthermore, the analysis was limited to static mechanical loading and did not incorporate cyclic fatigue, time-dependent bone remodeling, fracture healing processes, or long-term clinical outcomes. Consequently, the predicted stresses and displacements cannot be used to establish fatigue life, healing success, or clinical superiority of either fixation configuration.

Future research should explore more advanced material models to enhance the accuracy of biomechanical predictions. In vivo validation through clinical trials will also be crucial to confirm the applicability of these findings in surgical practice. Addressing these areas will contribute to a deeper understanding of miniplate fixation and further improve clinical outcomes in mandibular fracture treatment.

## 5. Conclusions

This study presents a comprehensive FEA of mandibular fracture fixation, evaluating the biomechanical performance of different miniplate configurations under realistic physiological loading. The findings emphasize the crucial role of plate geometry in optimizing stress distribution, reducing displacement, and improving overall fixation stability.

Under the investigated static loading conditions, the shorter, wider miniplate (20.5 × 3.5 × 1.25 mm) exhibited lower interfragmentary displacements and reduced stress concentrations compared with the longer, narrower configuration (27 × 2.5 × 1.25 mm). These findings indicate differences in the mechanical stabilization provided by the two configurations within the assumptions of the present finite element model.

However, the calculated interfragmentary displacements cannot be directly related to fracture healing outcomes, as the model does not account for the mechanical behavior of healing tissues or biological repair processes. Similarly, the predicted stress distributions do not provide sufficient evidence to assess fatigue failure or long-term implant durability.

Therefore, the findings should be interpreted as a comparative assessment of the static biomechanical behavior of the two fixation configurations rather than evidence of clinical superiority. Further experimental validation, cyclic loading investigations, and clinical studies are required to establish their long-term performance and clinical relevance.

The predicted molar reaction force reflects the prescribed literature-based muscle loading conditions and should not be considered independent validation of the model. Experimental validation is required before the quantitative predictions can be used to assess patient-specific postoperative biomechanical behavior.

**Author Contributions:** Conceptualization, V.D. and A.K.; methodology, A.K., V.D. and V.M.; validation, I.L. and L.L.; formal analysis, I.L., V.M. and V.D.; investigation, A.K., L.L. and I.L.; resources, V.D., I.L. and V.M.; data curation, V.D., L.L. and V.M.; writing—original draft preparation, A.K., V.D. and I.L.; writing—review and editing, L.L. and V.M.; visualization, A.K. and L.L.; supervision, A.K. and V.D.; project administration, A.K. and V.D. All authors have read and agreed to the published version of the manuscript.

**Funding:** This study was supported by the Ministry of Health of the Czech Republic (project MH CZ-DRO-VFN64165).

**Institutional Review Board Statement:** This study involved a retrospective computational analysis based on pre-existing, anonymized clinical CT data. No prospective patient recruitment, additional imaging, or clinical interventions were performed. The CT data were used exclusively for anatomical reconstruction and subsequent finite element modelling. No new clinical investigation involving human participants was conducted.

**Informed Consent Statement:** The medical imaging data were obtained from pre-existing clinical medical records and used retrospectively for secondary analysis. No additional examinations or interventions were performed specifically for this research. Patient consent was waived.

**Data Availability Statement:** Data are contained within the article.

**Conflicts of Interest:** The authors declare no conflicts of interest.

## References

1. Savani, R.; Hu, W.; Patel, S.; Shah, N.; Chauhan, S.; Chavda, Y. Effective strategies in the management of anterior mandibular fractures: A comprehensive systematic review. *Br. J. Oral Maxillofac. Surg.* **2024**, *62*, 349–360. [CrossRef] [PubMed]
2. Aşık, M.B.; Akay, S.; Eksert, S. Analyses of combat-related injuries to the maxillofacial and cervical regions and experiences in an operational field hospital. *Ulus. Travma Acil Cerrahi Derg.* **2018**, *24*, 56–60. [CrossRef] [PubMed]
3. Kidwai, S.M.; Lu, G.N. Mandibular body fractures. *Facial Plast. Surg. Clin. N. Am.* **2022**, *30*, 99–108. [CrossRef] [PubMed]
4. Skrypa, O.L.; Bandrivsky, Y.L. Determining the frequency of functional disorders of the TMJ in patients with mandible fractures depending on the location. *Wiad. Lek.* **2020**, *73*, 245–249. [CrossRef]
5. Yamamoto, K.; Matsusue, Y.; Horita, S.; Murakami, K.; Sugiura, T.; Kirita, T. Maxillofacial fractures associated with interpersonal violence. *J. Craniofac. Surg.* **2019**, *30*, e312–e315. [CrossRef] [PubMed]
6. Gibson, A.C.; Merrill, T.B.; Boyette, J.R. Complications of mandibular fracture repair. *Otolaryngol. Clin. N. Am.* **2023**, *56*, 1137–1150. [CrossRef] [PubMed]
7. Kovilpillai, F.J.; Royan, S.J.; Ma, B.C.; Gunarajah, D.R.; Adnan, T.H. A 4-year multicentre audit of complications following ORIF treatment of mandibular fractures. *J. Maxillofac. Oral Surg.* **2020**, *19*, 289–297. [CrossRef] [PubMed]
8. Gayathri, G.; Elavenil, P.; Sasikala, B.; Pathumai, M.; Krishnakumar, R.V.B. 'Stylo-mandibular complex' fracture from a maxillofacial surgeon's perspective—Review of the literature and proposal of a management algorithm. *Int. J. Oral Maxillofac. Surg.* **2016**, *45*, 297–303. [CrossRef] [PubMed]
9. Stanford-Moore, G.; Murr, A.H. Mandibular angle fractures. *Facial Plast. Surg. Clin. N. Am.* **2022**, *30*, 109–116. [CrossRef] [PubMed]
10. Khavanin, N.; Jazayeri, H.; Xu, T.; Pedreira, R.; Lopez, J.; Reddy, S.; Shamliyan, T.; Peacock, Z.S.; Dorafshar, A.H. Management of teeth in the line of mandibular angle fractures treated with open reduction and internal fixation: A systematic review and meta-analysis. *Plast. Reconstr. Surg.* **2019**, *144*, 1393–1402. [CrossRef] [PubMed]
11. Sobti, N.; Ahmed, K.S.; Polanco, T.; Chilov, M.; Cohen, M.A.; Boyle, J.; Shahzad, F.; Matros, E.; Nelson, J.A.; Allen, R.J. Mini-plate versus reconstruction bar fixation for oncologic mandibular reconstruction with free fibula flaps: A systematic review and meta-analysis. *J. Plast. Reconstr. Aesthet. Surg.* **2022**, *75*, 2691–2701. [CrossRef] [PubMed]
12. Mathew, N.; Singh, I.; Gandhi, S.; Solanki, M.; Bedi, N.S. The efficacy of fixation of unilateral mandibular angle fracture with single 3D plate vs single miniplate using transbuccal approach. *J. Maxillofac. Oral Surg.* **2022**, *21*, 405–412. [CrossRef] [PubMed]
13. Sukegawa, S.; Kanno, T.; Masui, M.; Sukegawa-Takahashi, Y.; Kishimoto, T.; Sato, A.; Furuki, Y. A retrospective comparative study of mandibular fracture treatment with internal fixation using reconstruction plate versus miniplates. *J. Craniomaxillofac. Surg.* **2019**, *47*, 1175–1180. [CrossRef] [PubMed]
14. Zhang, Q.; Wu, W.; Qian, C.; Xiao, W.; Zhu, H.; Guo, J.; Meng, Z.; Zhu, J.; Ge, Z.; Cui, W. Advanced biomaterials for repairing and reconstruction of mandibular defects. *Mater. Sci. Eng. C* **2019**, *103*, 109858. [CrossRef] [PubMed]

15. Elhadad, A.A.; Romero-Resendiz, L.; Rossi, M.C.; Rodríguez-Albelo, L.M.; Lascano, S.; Afonso, C.R.M.; Alcudia, A.; Amigó, V.; Torres, Y. Findings and perspectives of β-Ti alloys with biomedical applications: Exploring beyond biomechanical and biofunctional behaviour. *J. Mater. Res. Technol.* **2024**, *33*, 3550–3618. [CrossRef]
16. Weyh, A.M.; Quimby, A.; Fernandes, R.P. Three-dimensional computer-assisted surgical planning and manufacturing in complex mandibular reconstruction. *Atlas Oral Maxillofac. Surg. Clin.* **2020**, *28*, 145–150. [CrossRef] [PubMed]
17. Aftabi, H.; Zaraska, K.; Eghbal, A.; McGregor, S.; Prisman, E.; Hodgson, A.; Fels, S. Computational models and their applications in biomechanical analysis of mandibular reconstruction surgery. *Comput. Biol. Med.* **2024**, *169*, 107887. [CrossRef] [PubMed]
18. De Stefano, M.; Ruggiero, A. A critical review of human jaw biomechanical modeling. *Appl. Sci.* **2024**, *14*, 3813. [CrossRef]
19. Lisiak-Myszke, M.; Marciniak, D.; Bieliński, M.; Sobczak, H.; Garbacewicz, Ł.; Drogoszewska, B. Application of finite element analysis in oral and maxillofacial surgery—A literature review. *Materials* **2020**, *13*, 3063. [CrossRef] [PubMed]
20. Kondratiev, A.; Demenko, V.; Linetskiy, I.; Weisskircher, H.-W.; Linetska, L. Evaluation of bone turnover around short finned implants in atrophic posterior maxilla: A finite element study. *Prosthesis* **2024**, *6*, 1170–1188. [CrossRef]
21. Sancar, B.; Çetiner, Y.; Dayı, E. Evaluation of the pattern of fracture formation from trauma to the human mandible with finite element analysis. Part 2: The corpus and the angle regions. *Dent. Traumatol.* **2023**, *39*, 437–447. [CrossRef] [PubMed]
22. Meslier, Q.A.; Shefelbine, S.J. Using finite element modeling in bone mechanoadaptation. *Curr. Osteoporos. Rep.* **2023**, *21*, 105–116. [CrossRef] [PubMed]
23. Kondratiev, A.; Smetankina, N.; Staude, V. Biomechanical analysis of stress–strain distribution in the lumbar spine–sacrum–pelvis system with emphasis on sacroiliac joint dysfunction. *Prosthesis* **2025**, *7*, 4. [CrossRef]
24. Becheleni, M.T.; Souza, M.R.F.; Galvão, E.L.; Al-Moraissi, E.A.; Falci, S.G.M. Top 100 most-cited articles on mandibular fractures: A bibliometric analysis. *J. Oral Maxillofac. Surg.* **2023**, *81*, 878–891. [CrossRef] [PubMed]
25. Dogru, S.C.; Cansiz, E.; Arslan, Y.Z. A review of finite element applications in oral and maxillofacial biomechanics. *J. Mech. Med. Biol.* **2018**, *18*, 1830002. [CrossRef]
26. Merema, B.B.J.; Kraeima, J.; Glas, H.H.; Spijkervet, F.K.L.; Witjes, M.J.H. Patient-specific finite element models of the human mandible: Lack of consensus on current set-ups. *Oral Dis.* **2020**, *27*, 42–51. [CrossRef] [PubMed]
27. Linetskiy, I.; Sutcliffe, M.; Kondratiev, A.; Demenko, V.; Linetska, L.; Yefremov, O. A novel method of load-bearing ability analysis of short plateau implants placed in compromised bone. In Proceedings of the 2023 IEEE 4th KhPI Week on Advanced Technology (KhPIWeek), Kharkiv, Ukraine, 2–6 October 2023; pp. 1–6. [CrossRef]
28. Alaneme, K.K.; Kareem, S.A.; Ozah, B.N.; Alshahrani, H.A.; Ajibuwa, O.A. Application of finite element analysis for optimizing selection and design of Ti-based biometallic alloys for fractures and tissues rehabilitation: A review. *J. Mater. Res. Technol.* **2022**, *19*, 121–139. [CrossRef]
29. Jindal, P.; Worcester, F.; Walia, K.; Gupta, A.; Breedon, P. Finite element analysis of titanium alloy-graphene based mandible plate. *Comput. Methods Biomech. Biomed. Engin.* **2019**, *22*, 324–330. [CrossRef] [PubMed]
30. Prasadh, S.; Krishnan, A.V.; Lim, C.Y.H.; Gupta, M.; Wong, R. Titanium versus magnesium plates for unilateral mandibular angle fracture fixation: Biomechanical evaluation using 3-dimensional finite element analysis. *J. Mater. Res. Technol.* **2022**, *18*, 2064–2076. [CrossRef]
31. Daqiq, O.; Roossien, C.C.; Wubs, F.W.; van Minnen, B. Biomechanical assessment of mandibular fracture fixation using finite element analysis validated by polymeric mandible mechanical testing. *Sci. Rep.* **2024**, *14*, 11795. [CrossRef] [PubMed]
32. Orassi, V.; Duda, G.N.; Heiland, M.; Fischer, H.; Rendenbach, C.; Checa, S. Biomechanical assessment of the validity of sheep as a preclinical model for testing mandibular fracture fixation devices. *Front. Bioeng. Biotechnol.* **2021**, *9*, 672176. [CrossRef] [PubMed]
33. Kurakar, M.; Joshi, U. Comparative study of miniplate vs reconstruction plate in the management of bilateral parasymphysis mandible fracture: FEM analysis. *J. Maxillofac. Oral Surg.* **2023**, *22*, 9–17. [CrossRef] [PubMed]
34. Snyder, E.; Trabia, M.; Trabelsi, N. An approach for simultaneous reduction and fixation of mandibular fractures. *Comput. Methods Biomech. Biomed. Engin.* **2023**, *26*, 1064–1076. [CrossRef] [PubMed]
35. Shi, Q.; Sun, Y.; Yang, S.; Van Dessel, J.; Lübbers, H.-T.; Zhong, S.; Gu, Y.; Bila, M.; Politis, C. Preclinical study of additive manufactured plates with shortened lengths for complete mandible reconstruction: Design, biomechanics simulation, and fixation stability assessment. *Comput. Biol. Med.* **2021**, *139*, 105008. [CrossRef] [PubMed]
36. Shi, Q.; Sun, Y.; Yang, S.; Van Dessel, J.; Lübbers, H.-T.; Zhong, S.; Gu, Y.; Bila, M.; Dormaar, T.; Schoenaers, J.; et al. Failure analysis of an in-vivo fractured patient-specific Ti6Al4V mandible reconstruction plate fabricated by selective laser melting. *Eng. Fail. Anal.* **2021**, *124*, 105353. [CrossRef]
37. Zhong, S.; Shi, Q.; Sun, Y.; Yang, S.; Van Dessel, J.; Gu, Y.; Chen, X.; Lübbers, H.-T.; Politis, C. Biomechanical comparison of locking and non-locking patient-specific mandibular reconstruction plate using finite element analysis. *J. Mech. Behav. Biomed. Mater.* **2021**, *124*, 104849. [CrossRef] [PubMed]
38. Kondratiev, A.; Sutcliffe, M.; Demenko, V.; Linetskiy, I.; Yefremov, O.; Linetska, L. Efficiency of miniplates fixation in mandibular oblique fractures. In Proceedings of the 2024 IEEE 5th KhPI Week on Advanced Technology (KhPIWeek), Kharkiv, Ukraine, 7–11 October 2024; pp. 1–6. [CrossRef]

39. Heibel, H.; Alt, K.W.; Wächter, R.; Bähr, W. Cortical thickness of the mandible with special reference to miniplate osteosynthesis: Morphometric analysis of autopsy material. *Mund. Kiefer Gesichtschir* **2001**, *5*, 180–185. [CrossRef] [PubMed]
40. Zheng, F.; Zhu, Y.; Gong, Y.; Yin, D.; Liu, Y. Variation in stress distribution modified by mandibular material property: A 3D finite element analysis. *Comput. Methods Programs Biomed.* **2023**, *229*, 107310. [CrossRef] [PubMed]
41. Park, B.; Jung, B.T.; Kim, W.H.; Lee, J.-H.; Kim, B.; Lee, J.-H. The Stability of Hydroxyapatite/Poly-L-Lactide Fixation for Unilateral Angle Fracture of the Mandible Assessed Using a Finite Element Analysis Model. *Materials* **2020**, *13*, 228. [CrossRef] [PubMed]
42. Murakami, K.; Yamamoto, K.; Sugiura, T.; Horita, S.; Matsusue, Y.; Kirita, T. Computed Tomography-Based 3-Dimensional Finite Element Analyses of Various Types of Plates Placed for a Virtually Reduced Unilateral Condylar Fracture of the Mandible of a Patient. *J. Oral Maxillofac. Surg.* **2017**, *75*, 1239.e1–1239.e11. [CrossRef] [PubMed]
43. Ao Foundation. *Body, Simple*; AO Foundation: Davos, Switzerland, 2021.
44. Champy, M.; Loddé, J.P.; Schmitt, R.; Jaeger, J.H.; Muster, D. Mandibular osteosynthesis by miniature screwed plates via a buccal approach. *J. Maxillofac. Surg.* **1978**, *6*, 14–21. [CrossRef] [PubMed]
45. Synthes, DePuy. *MatrixMANDIBLE™ Plate and Screw System: Surgical Technique*; Document No. SE_807064 AF; Synthes GmbH: Oberdorf, Switzerland, 2022. Available online: https://www.jnjmedtech.com/en-EMEA/product/matrixmandible-plating-system (accessed on 16 November 2026).
46. Więckowski, W.; Motyka, M.; Adamus, J.; Lacki, P.; Dyner, M. Numerical and Experimental Analysis of Titanium Sheet Forming for Medical Instrument Parts. *Materials* **2022**, *15*, 1735. [CrossRef] [PubMed]
47. Cui, Y.-W.; Wang, L.; Zhang, L.-C. Towards load-bearing biomedical titanium-based alloys: From essential requirements to future developments. *Prog. Mater. Sci.* **2024**, *144*, 101277. [CrossRef]
48. Tate, G.S.; Ellis, E., III; Throckmorton, G. Bite forces in patients treated for mandibular angle fractures: Implications for fixation recommendations. *J. Oral Maxillofac. Surg.* **1994**, *52*, 734–736. [CrossRef] [PubMed]
49. Korioth, T.W.; Romilly, D.P.; Hannam, A.G. Three-dimensional finite element stress analysis of the dentate human mandible. *Am. J. Phys. Anthropol.* **1992**, *88*, 69–96. [CrossRef] [PubMed]
50. Oefner, C.; Herrmann, S.; Kebbach, M.; Lange, H.-E.; Kluess, D.; Woiczinski, M. Reporting checklist for verification and validation of finite element analysis in orthopedic and trauma biomechanics. *Med. Eng. Phys.* **2021**, *92*, 25–32. [CrossRef] [PubMed]
51. Demenko, V.; Linetskiy, I.; Linetska, L.; Sutcliffe, M.; Kondratiev, A. Prognosis of Crestally Placed Short Plateau Implants in Posterior Maxilla. *Int. J. Numer. Methods Biomed. Eng.* **2025**, *41*, e70025. [CrossRef] [PubMed]
52. Perren, S.M. Physical and biological aspects of fracture healing with special reference to internal fixation. *Clin. Orthop. Relat. Res.* **1979**, *138*, 175–196.
53. Champy, M.; Lodde, J.P. Étude des contraintes dans la mandibule fracturée chez l'homme. Mesures théoriques et vérification par jauges extensométriques in situ [Study of stresses in the fractured mandible in man. Theoretical measurement and verification by extensometric gauges in situ]. *Rev. Stomatol. Chir. Maxillofac.* **1977**, *78*, 545–551. [PubMed]
54. Pinheiro, M.; Willaert, R.; Khan, A.; Krairi, A.; Van Paepegem, W. Biomechanical evaluation of the human mandible after temporomandibular joint replacement under different biting conditions. *Sci. Rep.* **2021**, *11*, 14034. [CrossRef] [PubMed]
55. MacLeod, A.R.; Pankaj, P.; Simpson, A.H.R.W. Does Screw–Bone Interface Modelling Matter in Finite Element Analyses? *J. Biomech.* **2012**, *45*, 1712–1716. [CrossRef] [PubMed]
56. Çelik, T. Evaluation of the Relation Between Preload Values and Pull-Out Force of the Cortical Screw Used in Bone Fracture. *J. Biomech. Eng.* **2021**, *143*, 091008. [CrossRef] [PubMed]
57. Morgan, E.F.; Unnikrisnan, G.U.; Hussein, A.I. Bone mechanical properties in healthy and diseased states. *Annu. Rev. Biomed. Eng.* **2018**, *20*, 119–143. [CrossRef] [PubMed]
58. Apicella, D.; Aversa, R.; Ferro, F.; Ianniello, D.; Perillo, L.; Apicella, A. The importance of cortical bone orthotropicity, maximum stiffness direction and thickness on the reliability of mandible numerical models. *J. Biomed. Mater. Res. B Appl. Biomater.* **2010**, *93*, 150–163. [CrossRef] [PubMed]
59. Marangon, G.; Fincato, R.; Carniel, E.L.; Toniolo, I.; Berardo, A.; Mazzucco, G. Orthotropic reconstruction and characterization of bone tissues through a visco-plasto-damage model. *PLoS ONE* **2025**, *20*, e0335948. [CrossRef] [PubMed]


**Disclaimer/Publisher's Note:** The statements, opinions and data contained in all publications are solely those of the individual author(s) and contributor(s) and not of MDPI and/or the editor(s). MDPI and/or the editor(s) disclaim responsibility for any injury to people or property resulting from any ideas, methods, instructions or products referred to in the content.